arXiv:2107.13721v2 [stat.ML] 30 Jul 2021

Amplitude Mean of Functional Data on $\mathbb{S}^2$

Zhengwu Zhang
Department of Statistics and Operations Research
The University of North Carolina at Chapel Hill
zhengwu_zhang@unc.edu

Bayan Saparbayeva
Department of Neurology
University of Rochester Medical Center
bayan_saparbayeva@urmc.rochester.edu

January 23, 2022

Abstract

Mainfold-valued functional data analysis (FDA) recently becomes an active area of research motivated by the raising availability of trajectories or longitudinal data observed on non-linear manifolds. The challenges of analyzing such data comes from many aspects, including infinite dimensionality and nonlinearity, as well as time domain or phase variability. In this paper, we study the amplitude part of manifold-valued functions on $\mathbb{S}^2$, which is invariant to random time warping or re-parameterization of the function. Utilizing the nice geometry of $\mathbb{S}^2$, we develop a set of efficient and accurate tools for temporal alignment of functions, geodesic and sample mean calculation. At the heart of these tools, they rely on gradient descent algorithms with carefully derived gradients. We show the advantages of these newly developed tools over its competitors with extensive simulations and real data, and demonstrate the importance of considering the amplitude part of functions instead of mixing it with phase variability in mainfold-valued FDA.

Keywords— Spherical manifold Functional data Amplitude and phase Parallel transport Gradient descent

1 Introduction

Functional data analysis (FDA) has been an active area of research for decades, motivated by the rich availability of trajectories or longitudinal data observed over time. Well-known monographs include [22, 23, 3] and [5] among many others. Many advanced statistical techniques have been developed for classical functional data that take values in a vector space $p : [0,1] \to \mathbb{R}^d$, for instance, principal component analysis, functional linear regression and functional quantile regression (see [20, 7, 13]). However, many modern applications consider functional data taking values on a non-linear Riemannian manifold raised in the form $p : [0,1] \to \mathscr{M}$, where $\mathscr{M}$ is a Riemannian manifold. Compared with methods for vector valued functional data, analytical methods for functional data on non-linear Riemannian manifold are very limited. In this paper, we consider a special manifold $\mathscr{M} = \mathbb{S}^2$, and develop fundamental statistical tools, such as geodesic calculation, temporal alignment and sample mean and covariance calculation, for analyzing functional data on $\mathbb{S}^2$. Two examples of such data are shown in Figure 1, where the left panel shows migration paths of a type of bird called *Swainson hawk* and the right shows some tracks for hurricanes originated from the Atlantic ocean.

The challenges of analyzing functional data on a Riemannian manifold come from many aspects, such as infinite dimensionality and nonlinearity. While the infinite dimensionality property is easy to understand given the consideration is functional data, the nonlinearity challenge comes from the fact that the functions take values on a non-linear manifold space, making many advanced techniques relying on linear structure ineffective. Another important challenge is the time domain variability in the functional data, which is less often considered in the literature. Taking the bird migration tracks as an example, two birds can fly similar paths but with different speeds. This phenomenon is also presented in traditional functional data, e.g, the misaligned peaks in the biomechanical data presented in Figure 1.11 in [22], where alignment of the the functional data is necessary.

To more precisely describe the variability in the time domain, we start with introducing some notations. Let $p : [0,1] \mapsto \mathbb{S}^2$ denote a smooth function on the 2-sphere, and $\gamma : [0,1] \mapsto [0,1]$ be a positive diffeomorphism with $\gamma(0) = 0$

(a) Migration paths of Swainson hawk (b) Hurricanes in the Atlantic ocean

Figure 1: Examples of functional data on manifold. The left panel shows migration paths of a type of bird called Swainson hawk and the right shows some tracks for hurricanes originating in the Atlantic ocean.

and $\gamma(1) = 1$. Here the γ plays the role of re-parameterizing the functional data, that is $\tilde{p} = p(\gamma)$ is a re-parameterized version of p. p and $\tilde{p}$ have the same path on $\mathbb{S}^2$, but $p(t)$ can be significantly different from $\tilde{p}(t)$ for the same t. For any two smooth functions or trajectories $p_1, p_2 : [0,1] \mapsto \mathbb{S}^2$, to remove the re-parameterization variability, we often align them first, which is done through finding a γ such that $p_1(t)$ is optimally registered to $p_2(\gamma(t))$ for all $t \in [0,1]$. This problem can be extended to multiple functions $\{p_1, \ldots, p_n\}$ and we want to find a template and set of functions $\{\gamma_1, \ldots, \gamma_n\}$ so that the template and $\{p_1(\gamma_1), \ldots, p_1(\gamma_n)\}$ are optimally aligned. The template is regarded as amplitude mean and is our main consideration in this paper.

Classical statistical analysis of functional data on manifolds usually considers only raw amplitude variation (see [20, 22, 19, 7], and [13]) under some distance function, for example

$$d(p_1, p_2) = \int_0^1 d_g\big(p_1(t), p_2(t)\big)\mathrm{d}t, \tag{1}$$

where d_g is the geodesic distance function on a manifold $\mathscr{M}$. Utilizing this distance function, we can calculate summary statistics such as mean and covariance on the tangent space of the mean (see [13, 14]). However, due to the presence of the phase variability, the mean based on (1) does not always reflect the common pattern of the data and the covariance is inflated, as illustrated later in the real data analysis. Alignment or phase-amplitude separation is an important step in manifold-valued FDA.

Structural analysis was proposed in [9] to align curves by identifying the timing of salient features before applying further statistics. Another alignment method is the Procrustes method (see [21]) that iteratively warps each curve to the sample Fréchet mean. The alignment is performed with the help of dynamic time warping algorithms (see [1, 6, 8, 24, 28]), e.g., synchronizing two functions p_1, p_2 with respect to some distance function

$$d(p_1, p_2) = \inf_{\gamma \in \Gamma} \int_0^1 d_g\Big(p_1(t), p_2\big(\gamma(t)\big)\Big)\mathrm{d}t, \tag{2}$$

where Γ is the set of positive diffeomorphisms $\Gamma = \big\{\gamma \in \mathrm{Diff}([0,1]) : \gamma(0) = 0,\ \gamma(1) = 1\big\}$. However, due to the fact that the distance function (1) is not invariant under the group of re-parameterization Γ, the objective function (2) has the vanishing effect ([15, 18, 16]). Sobolev metrics (see [17, 27, 29]) overcome these issues but are not always easy to compute. In [29], the importance of the fact that the distance function should be invariant under the Lie group of actions was elaborated.

A few recent studies start to develop more appropriate metrics and distance functions to perform FDA on manifold. Leveraging advancements in shape analysis, [26] extended the square-root velocity curve in the Euclidean space [25] to the manifold by parallel transporting all square-root velocity vectors to some reference point $c \in \mathscr{M}$ along geodesic paths

$$q(t) = \left(\frac{\dot{p}(t)}{\sqrt{|\dot{p}(t)|}}\right)^{||}_{p(t) \to c}.$$

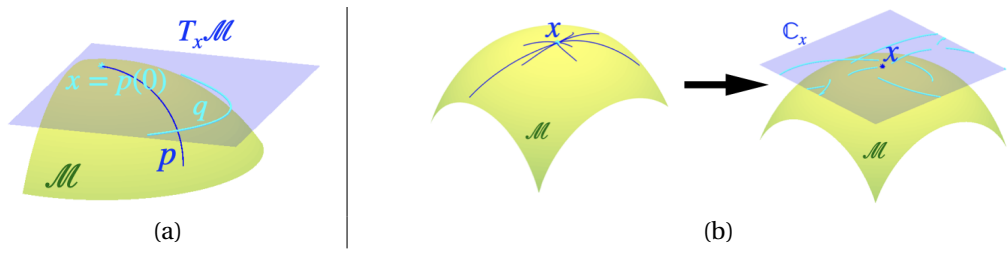

Figure 2: Panel (a) illustrates using (x, q) to represent a function p on $\mathbb{S}^2$, and panel (b) shows the space $\mathbb{C}_x$ containing all absolutely continuous functions that start at x. Here we have $\mathcal{M} = \mathbb{S}^2$.

Although this generalization makes the distance function invariant under Γ, the random choice of the reference point $c \in \mathcal{M}$ can introduce distortions and uncertainty into the analysis. To overcome the need of choosing an arbitrary reference point and transforming the functions on the manifold to a Euclidean space, more intrinsic methods were proposed in [30, 31, 12, 4], where they treat the manifold-valued functions as an (infinite-dimensional) manifold itself, and equip it with a Riemannian metric that can be invariant with respect to re-parameterization of functions. However, due to the complexity of the proposed metrics and the manifold itself, these methods all have significant computational challenges to calculate geodesics and amplitude mean after alignment.

In this work, we adopt the representation framework in [30] to inherit its advantages in analyzing FDA on manifolds, and develop a set of efficient and accurate tools for analyzing the amplitude mean of functional data on $\mathbb{S}^2$. The most important contribution of this paper is a gradient descent algorithm for more effectively computing the geodesic between the amplitudes of two functions on $\mathbb{S}^2$. To achieve this, we have to invent novel computational tools and algorithms. More specifically, compared with [30], this paper's novel contributions include: 1) we explicitly derive the analytical formulas for parallel transport along any circular arc β, where in [30] the parallel transports along β are compromised by numerical approximation; 2) we develop an efficient and accurate gradient descent method to obtain the geodesic between two elements on $\mathbb{C}$, where $\mathbb{C}$ represents the set of all functional data in our framework; and 3) the semi-linearity of $\mathbb{C}$ is utilized to simplify the geodesic calculation. The proposed new tools have been implemented in Matlab (source code can be found on GitHub `https://github.com/Bayan2019/2DSphericalTrajectories`), and compared with the tools in [30] in both simulated and real-world data to demonstrate their advantages.

The rest of the paper is organized as follows. In sections 2 and 3 the Riemannian geometry of smooth functions on $\mathbb{S}^2$ is introduced. It is worth to notice that Theorem 2.1 is an extended version of Theorem 1 in [30]. In section 4, we show how to calculate the sample Fréchet mean for a set of functional data and their amplitudes, and study asymptotic properties of the sample Fréchet mean. In sections 5 and 6 we present simulation studies and real data analyses, respectively. Section 7 concludes the paper.

2 Riemannian Geometry of Smooth Functions on $\mathbb{S}^2$

Let $p : [0,1] \mapsto \mathbb{S}^2$ denote a smooth function on the 2-sphere, and let the set of all such functions be denoted as $\mathcal{F} = \{p : [0,1] \mapsto \mathbb{S}^2 | p \text{ is smooth}\}$. Also, Γ is the set of positive diffeomorphisms $\Gamma = \left\{\gamma \in \mathrm{Diff}([0,1]) : \gamma(0) = 0,\ \gamma(1) = 1\right\}$. Γ forms a group action under the composition: $\mathcal{F} \times \Gamma \mapsto \mathcal{F}$ according to $p \circ \gamma \mapsto p(\gamma)$, where p and $p(\gamma)$ follow the same trajectory on $\mathbb{S}^2$ but with different phase (temporal evaluation speed). We represent the function p using its starting point and a transported square-root vector curve (TSRVC):

$$x = p(0) \in \mathbb{S}^2, \qquad q(t) = \left(\frac{\dot{p}(t)}{\sqrt{|\dot{p}(t)|}}\right)^{\|}_{p(t)\to x=p(0)} \in T_x\mathbb{S}^2,$$

where $(v)^{\|}_{p(t)\to x}$ represents parallel transport of vector $v \in T_{p(t)}\mathbb{S}^2$ to $T_x\mathbb{S}^2$, and the parallel transport is done along the curve itself $p(t)$. Note that $q(t)$ is a function in $T_x\mathbb{S}^2$. We represent p using a pair (x, q), illustrated in Figure 2 (a). The TSRVC representation is bijective: any $p \in \mathcal{F}$ can be uniquely represented by a pair (x, q) and we can reconstruct p from (x, q) using covariant integral [31]. When it is convenient, we use $p = (x, q)$ for notation simplicity and we will explicitly point out the notation change.

First of all, for any $x \in \mathbb{S}^2$ we have $\mathbb{C}_x = \mathbb{L}_2([0,1], T_x\mathbb{S}^2)$ to represent all absolutely continuous functions or trajectories on $\mathbb{S}^2$ that start at x. Namely, we consider a smooth trajectory $p : [0,1] \to \mathbb{S}^2$ that starts at $p(0) = x$ as an element in $\mathbb{C}_x$

$$q(t) = \left(\frac{\dot{p}(t)}{\sqrt{|\dot{p}(t)|}}\right)^{\|}_{p(t)\to x} \in \mathbb{C}_x.$$

So the full space of interest becomes a bundle

$$\mathbb{C} = \bigsqcup_{x\in\mathbb{S}^2} \mathbb{C}_x,$$

which is similar to the tangent bundle $T\mathbb{S}^2$ but instead of tangent vectors we consider square-integrable functions on tangent spaces. For the manifold $\mathbb{C}$ we have the following tangent space

$$T_{(x,q)}\mathbb{C} = T_x\mathbb{S}^2 \bigoplus \mathbb{C}_x,$$

and define the inner product

$$\big\langle (u_1, w_1), (u_2, w_2)\big\rangle_{(x,q)} = \langle u_1, u_2\rangle_x + \int_0^1 \langle w_1(t), w_2(t)\rangle_x \mathrm{d}t, \tag{3}$$

where $(u_i, w_i) \in T_{(x,q)}\mathbb{C}$, and $\langle\cdot,\cdot\rangle_x$ is a scalar product in $T_x\mathbb{S}^2$.

Our main focus is the amplitude of functions, i.e., the quotient space $\mathbb{C}/\Gamma$. However, since the distance function on $\mathbb{C}/\Gamma$ is determined through the distance function on $\mathbb{C}$, we have to review the geometry of $\mathbb{C}$ first. As for all Riemannian manifolds, the distance between two elements $(x_0, q_0), (x, q) \in \mathbb{C}$ is determined by the length of geodesic curve, i.e., the shortest path

$$\big(\beta(s), q(s,\cdot)\big) \in \mathbb{C}$$

connecting (x_0, q_0) and (x, q) with

$$\big(\beta(0) = x_0, \quad q(0,\cdot) = q_0\big) \quad \text{and} \quad \big(\beta(1) = x, \quad q(1,\cdot) = q\big).$$

Proposition 1. If a path $\big(\beta(s), q(s,\cdot)\big)$ is geodesic on $\mathbb{C}$ under the metric (3), then it satisfies the following properties:

1. the base-curve $\beta(s)$ is constant-speed parameterized;
2. TSRVC $q(s,\cdot)$ is covariantly linear along β, and that is, $\nabla_{\dot\beta(s)}\big(\nabla_{\dot\beta(s)} q(s,t)\big) = 0$.

Proof. The proof can be found in [6]. □

If a path on $\mathbb{C}$ satisfies the two properties listed above, then it is completely determined by the curve $\beta \in \mathbb{S}^2$, which is called the *base-curve* in the following context. That is, once we fix $\beta(s)$, we have $q(s,t) = q^{||}_{0,\beta(s)}(t) + s\big(q^{||}_{\beta(s)}(t) - q^{||}_{0,\beta(s)}(t)\big)$, where $q^{||}_{0,\beta(s)}(t)$ is the parallel transport of $q_0(t)$ from $\beta(0)$ to $\beta(s)$ along β for $s \in [0,1]$, and $q^{||}_{\beta(s)}(t)$ is the parallel transport of $q(t)$ from $\beta(1)$ to $\beta(s)$ along β. Moreover, the length of this path is defined as

$$d_\beta(p_0, p) = d_\beta((x_0, q_0), (x, q)) = \sqrt{\ell^2_\beta + \int_0^1 \big|q^{||}_{0,\beta(1)}(t) - q(t)\big|^2 \mathrm{d}t}, \tag{4}$$

where $\ell^2_\beta = \Big(\int_0^1 \sqrt{\langle\dot\beta(t), \dot\beta(t)\rangle_{\beta(t)}}\mathrm{d}t\Big)^2 = |\dot\beta(0)|^2$. If a path $(\beta(s), q(s,\cdot))$ is not a geodesic on $\mathbb{C}$, we can still use equation (4) to quantify its length. If β is unknown, we find the geodesic distance according to

$$d_{\mathbb{C}}(p_0, p) = \min_\beta d_\beta\big(p_0, p\big). \tag{5}$$

The following theorem presents the main advantage of using TSRVC.

Theorem 1. For any two trajectories $p_0, p \in \mathscr{F}$, and their corresponding TSRVC representations $(x_0, q_0), (x, q) \in \mathbb{C}$, any smooth base-curve β, and any re-parameterization $\gamma \in \Gamma$, there is equality

$$d_\beta\big(p_0, p\big) = d_\beta\big(p_0(\gamma(t)), p(\gamma(t))\big) = d_\beta\Big(\big(x_0, q_0(\gamma(t))\sqrt{\dot\gamma(t)}\big), \big(x, q(\gamma(t))\sqrt{\dot\gamma(t)}\big)\Big).$$

The proof of this theorem is presented in the supplement. This theorem highlights the advantage of using TSRVC representation to study functional data or trajectories on $\mathbb{S}^2$: the action of Γ on $\mathbb{C}$ under the metric d_β is by isometries. The isometry property of re-parameterization allows us to focus on the amplitude of a function and analyze it in a manner that is invariant to random time warping.

To represent the amplitude of a function, we first introduce a closed set $\tilde\Gamma$, containing all non-decreasing, absolutely continuous functions γ on $[0,1]$ such that $\gamma(0) = 0$ and $\gamma(1) = 1$. It can be shown that Γ is a dense subset of $\tilde\Gamma$ and the orbit of a TSRVC under $\tilde\Gamma$, defined as $[p] := (x, [q]) = \big\{\big(x, q(\gamma)\sqrt{\dot\gamma}\big) \big| \gamma \in \tilde\Gamma\big\}$, forms a closed set (which is not the case under Γ). For theory development, we utilize $\tilde\Gamma$, and define the function amplitudes as the set of orbits under the group action $\tilde\Gamma$: $\mathbb{C}/\tilde\Gamma = \{(x, [q]) | (x, q) \in \mathbb{C}\}$. In practice, we will only use elements in Γ for simplicity. According to Theorem 1, we define the distance between amplitudes on $\mathbb{C}/\tilde\Gamma$ as

$$d_{\mathbb{C}/\tilde\Gamma}([p_0], [p]) = \min_{\gamma_1,\gamma_2\in\tilde\Gamma} d_{\mathbb{C}}(p_0\circ\gamma_1, p\circ\gamma_2) \approx \min_{\gamma\in\Gamma} d_{\mathbb{C}}(p_0, p\circ\gamma) \quad . \tag{6}$$

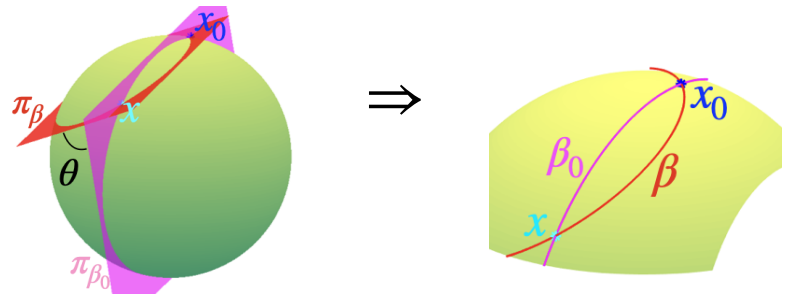

(a) (b)

Figure 3: Illustration of p-optimal curve β connecting x and x_0. Panel (a) shows two planes π_β and π_{β_0} containing x_0 and x on $\mathbb{S}^2$. The interaction between $\mathbb{S}^2$ and π_β contains a circular arc β and the interaction between $\mathbb{S}^2$ and π_{β_0} gives β_0, which is the geodesic on $\mathbb{S}^2$ between x_0 and x. Panel (b) shows β and β_0.

3 Geodesic Computation between Smooth Functions on $\mathbb{S}^2$

We now study how to obtain the geodesic between two elements on $\mathbb{C}$ and $\mathbb{C}/\tilde{\Gamma}$. Proposition 1 describes two important properties about the geodesic path, which will help us to find the geodesic.

3.1 Geometry of base-curve β

To understand the geometry of base-curve β, we start with introducing the concept named *p-optimal curves*. A curve β connecting two points x_0 and x on $\mathbb{S}^2$ is called p-optimal if $\ell_\beta \le \ell_\eta$, where ℓ_η is the length of η, and η is any curve that connects x_0 and x with the parallel transport map from $T_{x_0}\mathbb{S}^2$ to $T_x\mathbb{S}^2$ equal to the parallel transport map along β from $T_{x_0}\mathbb{S}^2$ to $T_x\mathbb{S}^2$ (see the detailed definition in [30]). With this p-optimal concept in mind, we have the following lemmas.

Lemma 1. If a path $\big(\beta(s), q(s,\cdot)\big)$ on $\mathbb{C}$ is a geodesic, then the base-curve β is a p-optimal curve.

Proof. Let us assume that we can find a shorter curve than β from x_0 to x that induces the same parallel transport from $T_{x_0}\mathbb{S}^2$ to $T_x\mathbb{S}^2$, then we can reduce ℓ_β without affecting $\int_0^1 \left|q^{||}_{0,\beta(1)}(t) - q(t)\right|^2 \mathrm{d}t$. Hence $\big(\beta(\cdot), q(\cdot,t)\big)$ does not have the shortest distance, and therefore it would not be a geodesic on $\mathbb{C}$. So there is a contradiction. □

Lemma 2. For any two points $x_0, x \in \mathbb{S}^2$, the only p-optimal curves connecting them on $\mathbb{S}^2$ are the circular arcs.

Proof. Let β be the curve joining x_0 with x on $\mathbb{S}^2$, and $\mathscr{P}(\beta)_0^1 : T_{x_0}\mathbb{S}^2 \to T_x\mathbb{S}^2$ be the parallel translation map induced by β. Let a circle passing x_0 and x on $\mathbb{S}^2$ be $\zeta = \zeta_1 \cup \zeta_2$, where ζ_1 is the circular arc from x_0 to x that induces the same parallel transport $\mathscr{P}(\beta)_0^1$ as β. The Gauss Bonnet theorem states that the angle of rotation of the parallel transport map $T_{x_0}\mathbb{S}^2 \to T_{x_0}\mathbb{S}^2$ induced by the closed curve ζ is equal of the integral of the Gaussian curvature over the region enclosed by the loop ζ. Since the Gaussian curvature of $\mathbb{S}^2$ equals $+1$ at every point, the angle of rotation is equal to the area enclosed by ζ. So the circle ζ has the shortest distance among all loops with the same parallel transport map. Therefore $\ell_\beta + \ell_{\zeta_2} \ge \ell_{\zeta_1} + \ell_{\zeta_2}$. Hence $\beta = \zeta_1$. □

The two lemmas significantly reduce the search space for the base-curve β in the geodesic calculation between two elements (x_0, q_0) and (x, q) on $\mathbb{C}$, i.e., the base-curve β must be among the circular arcs connecting x_0 and x on $\mathbb{S}^2$.

Now let us consider how to construct circular arcs connecting x_0 and x on $\mathbb{S}^2$. We start with constructing a plane π_β containing x_0 and x (refer to the red plane in Figure 3 panel (a)). The plane π_β is determined by its normal vector n (a vector orthogonal to π_β). We construct vector n based on an angle $\theta \in \left[-\frac{\pi}{2}, \frac{\pi}{2}\right]$ between n and the cross product of x_0 and x, defined as $x_0 \times x$. When we vary θ, we get different n, and thus π_β, and the intersection between π_β and $\mathbb{S}^2$. n has the following explicit expression as a function of θ:

$$n(\theta; x_0, x) = \frac{x_0 + x}{|x_0 + x|}\sin\theta + \frac{x_0 \times x}{|x_0 \times x|}\cos\theta.$$

The intersections between π_β and $\mathbb{S}^2$ give p-optimal curves with the following explicit expression:

$$\beta(s;\theta) = x_0\cos(s\phi) + (n \times x_0)\sin(s\phi) + n\langle n, x_0\rangle\big(1 - \cos(s\phi)\big), \tag{7}$$

where $\phi = 2\arcsin\left(\frac{1}{2}\sqrt{\frac{2-2\langle x_0,x\rangle}{1-\langle n,x_0\rangle^2}}\right)$, and n is determined by θ. For notation simplicity, $\beta(s;\theta)$ is also denoted as $\beta(\theta)$ or β when there is no confusion. Figure 3 panel (b) illustrates a circular arc β and the geodesic β_0 between x_0 and x on $\mathbb{S}^2$. Note that according to equation (7), the circular arcs between x_0 and x are parameterized by a single parameter θ and have a closed form solution, which allows us to derive an efficient optimization algorithm to find the geodesic base-curve β.

3.2 Geodesic calculation on $\mathbb{C}$

For two smooth functions p_0 and p on $\mathbb{S}^2$, their geodesic distance can be calculated using formula (5), and the geodesic is completely determined by the base-curve β. With the help of the two lemmas in section 3.1, we have significantly reduced the search domain of β and can represent it using only one parameter θ. Now we rewrite the geodesic distance calculation as a function of θ:

$$d^2_{\mathbb{C}}(p_0,p) = \min_{\theta\in\left[-\frac{\pi}{2},\frac{\pi}{2}\right]} d^2(p_0,p,\theta) = \min_{\theta\in\left[-\frac{\pi}{2},\frac{\pi}{2}\right]} \ell^2_{\beta(\theta)} + \int_0^1 \left|q^{||}_{0,\beta(\theta)}(t) - q(t)\right|^2 \mathrm{d}t.$$

One very attractive property of the p-optimal base-curve constructed according to equation (7) is that we have explicit expressions for $\ell_{\beta(\theta)}$ and the parallel transport $q^{||}_{0,\beta(\theta)}(t)$ as functions of θ. We refer the readers to the Propositions 1 and 2 in the supplement for detailed derivations.

To summarize, the distance function $d(p_0,p,\theta)$ depends on θ that determines the base-curve $\beta(\theta)$. Therefore, to get $d^2_{\mathbb{C}}(p_0,p)$, we can obtain $\frac{\partial}{\partial\theta}d^2(p_0,p,\theta)$, and rely on the gradient descent method to find the optimal θ. Fortunately, on $\mathbb{S}^2$, we also can obtain an explicit solution for the gradient, which is presented in section 3 in the supplement. We derive Algorithm 1 to find $\theta(p_0,p) = \operatorname{argmin}_{\theta\in\left[-\frac{\pi}{2},\frac{\pi}{2}\right]} d^2(p_0,p,\theta)$.

Algorithm 1: The method for finding geodesical $\theta(p_0,p)$

Input: two smooth functions p_0 and p, $\theta_0 \in \left[-\frac{\pi}{2},\frac{\pi}{2}\right]$, the gradient step $\lambda\in\mathbb{R}$, and the degree of accuracy $\varepsilon\in\mathbb{R}_+$
Output: a point $\theta\in\left[-\frac{\pi}{2},\frac{\pi}{2}\right]$
begin
  Set $\theta = \theta_0$.
  repeat
    Compute $\bar{\theta} = \theta - \lambda\frac{\partial}{\partial\theta}d^2(p_0,p,\theta)$.
    if $\bar{\theta}\in\left[-\frac{\pi}{2},\frac{\pi}{2}\right]$ and $d^2(p_0,p,\bar{\theta}) < d^2(p_0,p,\theta)$ **then**
      $\theta = \theta - \lambda\frac{\partial}{\partial\theta}d^2(p_0,p,\theta)$;
    else
      $\lambda = \frac{\lambda}{2}$;
  until $\left|\frac{\partial}{\partial\theta}d^2(p_0,p,\theta)\right| < \varepsilon$;

Finally, after finding the optimal $\theta(p_0,p)$, we build the geodesic path as

$$\beta(s) = \beta(s;\theta(p_0,p)) \qquad \text{and} \qquad q(s,t) = q^{||}_{0,\beta(s)}(t) + s\left(q^{||}_{\beta(1-s)}(t) - q^{||}_{0,\beta(s)}(t)\right).$$

Figure 4 shows one example of p_0 and p on $\mathbb{S}^2$, $d^2(p_0,p,\theta)$ and its derivative $\frac{\partial}{\partial\theta}d^2(p_0,p,\theta)$, the base-curve β and the final geodesic path between p_0 and p.

3.3 The exponential and inverse exponential maps on $\mathbb{C}$

For statistical analysis of a set of observations on $\mathbb{C}$, two other important tools are the exponential and inverse exponential maps. Let $(u,w)\in T_{(x,q)}\mathbb{C}$, the exponential map $\exp_{(x,q)}(s(u,w))$ is a mapping from $T_{(x,q)}\mathbb{C}$ to $\mathbb{C}$, and gives a geodesic $(\beta(s),q(s,t))$ on $\mathbb{C}$, where $s\in[0,1]$. Given p_0 and p on $\mathbb{S}^2$, and their TSRVC representations (x_0,q_0) and (x,q), the inverse exponential map $\exp^{-1}_{(x_0,q_0)}(x,q)$ gives a tangent vector (u,w) on $T_{(x_0,q_0)}\mathbb{C}$, such that $\exp_{(x_0,q_0)}((u,w)) = (x,q)$. Since we consider p and (x,q) as the same, for notation simplicity $\exp_p(s(u,w))$ is also used to denote the exponential map from $T_p\mathbb{C}$ to $\mathbb{C}$ and $\exp^{-1}_{p_0}p$ to denote for the inverse exponential map from $\mathbb{C}$ to $T_{p_0}\mathbb{C}$.

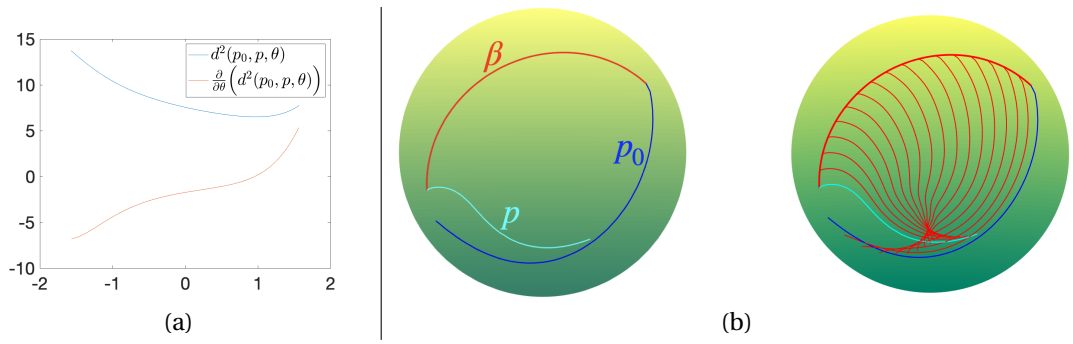

Figure 4: Panel (a) shows $d^2(p_0,p,\theta)$ with its derivative $\frac{\partial}{\partial\theta}d^2(p_0,p,\theta)$. Panel (b) left side shows the base-curve β which determines the geodesic on $\mathbb{C}$ between p_0 and p, and the right side shows the geodesic between p_0 and p.

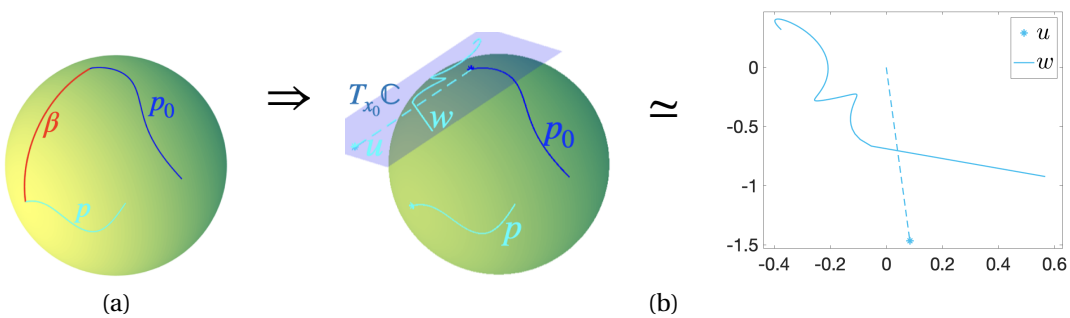

Figure 5: Panel (a) shows the base-curve β which determines the geodesics on $\mathbb{C}$ between two functions p_0 and p,. Panel (b) shows $(u,w)=\exp_{p_0}^{-1}p$ on the tangent space $T_{x_0}\mathbb{S}^2$.

On $\mathbb{C}$, once we find the optimal geodesic $\theta\in\left[-\frac{\pi}{2},\frac{\pi}{2}\right]$ for p_0 and p by Algorithm 1, it is straightforward to get the inverse exponential map

$$\exp_{p_0}^{-1}p=\left(\dot\beta(0;\theta),q_\beta^{||}-q_0\right), \tag{8}$$

where β is determined by θ. Figure 5 shows one example of p_0 and p on $\mathbb{S}^2$ and the inverse exponential map $\exp_{p_0}^{-1}p$.

The exponential mapping $\exp_{p_0}((u,w))$ is harder to compute than the inverse exponential map. Let $(\beta(s),q(s,\cdot))=\exp_{p_0}(s(u,w))$ for $s\in[0,1]$. We need to construct a $(\beta(s),q(s,\cdot))$ that satisfies the two properties in Proposition 1 and $\dot\beta(0)=u$. We describe our procedure to construct such $(\beta(s),q(s,\cdot))$ as follows.

For a given $u\in T_{x_0}\mathbb{S}^2$, we can construct a set of p-optimal curves determined by a set of planes π_β that intersect with $T_{x_0}\mathbb{S}^2$ by the line x_0+tu for $t\in\mathbb{R}$, where π_β is determined by a normal vector

$$n(\vartheta;x_0,u)=x_0\cos\vartheta+\frac{x_0\times u}{|x_0\times u|}\sin\vartheta \qquad \text{for} \quad \vartheta\in\left(\arcsin\left(\frac{|u|}{\pi}\right),\pi-\arcsin\left(\frac{|u|}{\pi}\right)\right). \tag{9}$$

One can find out that

$$\begin{aligned}&\beta(s;\vartheta)=x_0\cos(s\phi)+(n\times x_0)\sin(s\phi)+n\langle n,x_0\rangle\left(1-\cos(s\phi)\right) \qquad \text{with} \quad \phi(\vartheta)=\frac{|u|}{\sin\vartheta},\\ &q(s,t)=\left(sw(t)+q_0(t)\right)_{\beta(s)}^{||}.\end{aligned} \tag{10}$$

It is easy to see that the above path (10) satisfies the two properties in Proposition 1. By setting $s=1$, we get the end point $p=\exp_{p_0}\left((u,w)\right)$ with

$$p=(x,q) \qquad \text{where} \qquad \begin{aligned}&x=x_0\cos\phi+(n\times x_0)\sin\phi+n\langle n,x_0\rangle(1-\cos\phi),\\ &q=(w+q_0)_\beta^{||}.\end{aligned}$$

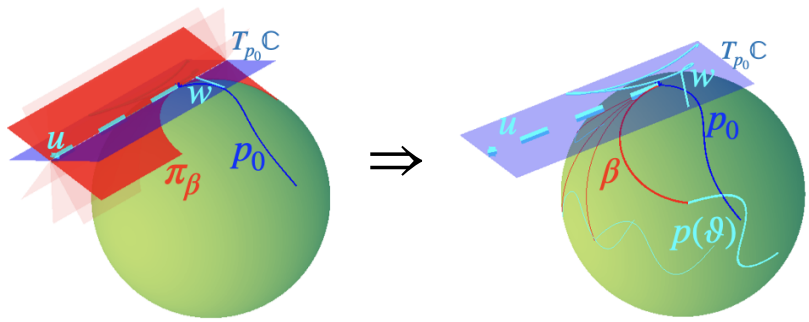

(a) (b)

Figure 6: Illustration on how to compute $\exp_{p_0}((u,w))$. Panel (a) shows a set of planes π_β containing the vector $u \in T_x\mathbb{S}^2$, and panel (b) shows $\beta(s;\vartheta)$ (the interactions between π_β and $\mathbb{S}^2$) and p which are also parameterized by ϑ.

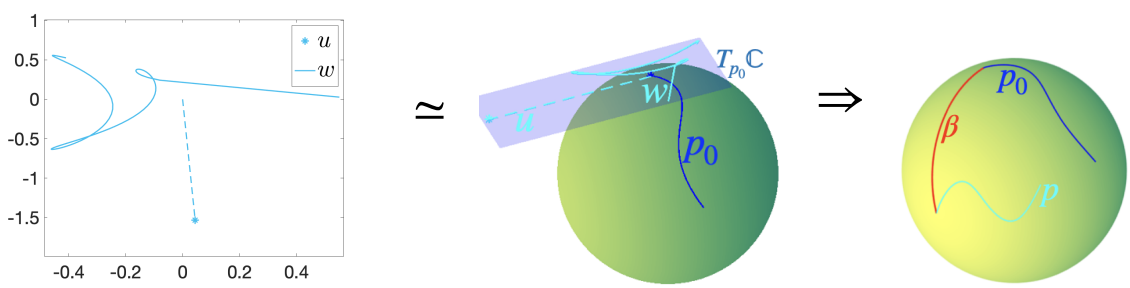

(a) (b)

Figure 7: Panel (a) illustrates an element $(u,w) \in T_{p_0}\mathbb{C}$, where u is a vector and w is a smooth function. Panel (b) shows $p = \exp_{p_0}((u,w))$ and the base-curve β.

Figure 6 panel (a) illustrates a set of planes π_β that contain the vector $u \in T_x\mathbb{S}^2$ (parameterized by ϑ with normal vectors in (9)), and panel (b) shows $\beta(s;\vartheta)$ and p which are also parameterized by ϑ.

To this end the challenge is to find an appropriate ϑ, such that the angle $\theta(\vartheta) = \arcsin\left(\sqrt{\frac{2}{1+\langle x_0,x\rangle}}\cos\vartheta\right)$ is optimal for p_0 and p, i.e., the base-curve β gives the smallest distance between p_0 and p. We then derive a gradient descent method to find the optimal $\vartheta \in \left(\arcsin\left(\frac{|u|}{\pi}\right), \pi - \arcsin\left(\frac{|u|}{\pi}\right)\right)$ in Algorithm 7 in the supplement.

3.4 Geodesic calculation between the amplitudes of functions on $\mathbb{C}/\Gamma$

Now we consider the amplitude of smooth functions on $\mathbb{S}^2$, which is defined as elements in the quotient space $\mathbb{C}/\tilde{\Gamma}$, e.g., $[p_0],[p] \in \mathbb{C}/\tilde{\Gamma}$. Formula (6) is used to calculate the geodesic distance between $[p_0]$ and $[p]$. In this case, we have a bivariate optimization problem: in addition to θ, we need to find a time warping function γ to minimize the distance between two orbits $[p_0]$ and $[p]$. We adopt a coordinate descent approach to iteratively solve the single variable optimization problems: (i) given θ, we solve γ using the Dynamic Programming algorithm in [1]: $\gamma = \operatorname{argmin}_{\gamma\in\Gamma} d^2(p_0\circ\gamma, p, \theta)$; and (ii) given γ, we solve θ based on the Algorithm 1.

We use following Algorithm 2 to find the base-curve β^* on $\mathbb{C}/\Gamma$ and the optimal time warping γ^* to align p_0 to p.

It is important to notice that the geodesic base-curve β^* in the space of function amplitudes $\mathbb{C}/\Gamma$ can be different from the geodesic base-curve β on $\mathbb{C}$. Figure 8 shows two examples of p_0 and p on $\mathbb{S}^2$, the base-curve β in $\mathbb{C}$, the base-curve β^* in $\mathbb{C}/\Gamma$, the geodesic path between p_0 and p in $\mathbb{C}/\Gamma$, and the optimal γ^* for aligning p_0 to p.

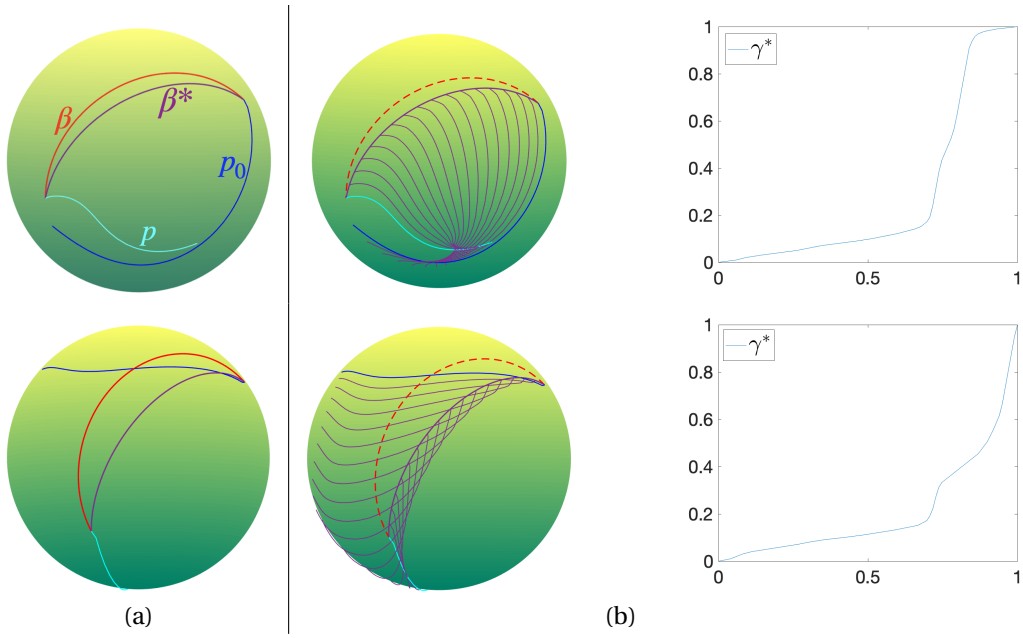

Figure 8: Comparison of base-curves β (for geodesics on $\mathbb{C}$) and β^* (for geodesics on $\mathbb{C}/\Gamma$). Panel (a) shows two examples of p, p_0 and the geodesic base-curves β and β^*. Panel (b) shows the geodesics between amplitudes of functions on $\mathbb{C}/\Gamma$ with the corresponding time warping functions $\gamma^* \in \Gamma$ on the right.

Algorithm 2: The method for finding geodesical $\theta^*([p_0],[p])$ and γ^* in $\mathbb{C}/\Gamma$

Input: two smooth functions $p_0, p, \theta_0 \in \left[-\frac{\pi}{2}, \frac{\pi}{2}\right]$, the gradient step $\lambda \in \mathbb{R}$, and the degree of accuracy $\varepsilon \in \mathbb{R}$

Output: a point $\theta^* \in \left[-\frac{\pi}{2}, \frac{\pi}{2}\right]$ and the re-parameterization $\gamma^* \in \Gamma$

begin

Set $\theta^* = \theta_0$. Find $\gamma^* = \arg\min_{\gamma\in\Gamma} d^2(p_0, p, \theta^*)$. Then get $\tilde{p}_0 = p_0 \circ \gamma^*$.

repeat

Compute θ^* based on Algorithm 1 with input $(\tilde{p}_0, p, \theta^*, \lambda, \varepsilon)$.

Find $\gamma^* = \operatorname{argmin}_{\gamma\in\Gamma} d^2(p_0, p, \theta^*)$. Update $\tilde{p}_0 = p_0 \circ \gamma^*$.

until $\left|\frac{\partial}{\partial\theta} d^2(\tilde{p}_0, p, \theta^*)\right| < \varepsilon$;

4 The Sample Fréchet Means on $\mathbb{C}$ and $\mathbb{C}/\tilde{\Gamma}$

With a clear understanding of the geometry of $\mathbb{C}$ and $\mathbb{C}/\tilde{\Gamma}$, we now are ready to study the Fréchet means of smooth functions on $\mathbb{S}^2$ (elements on $\mathbb{C}$) and their amplitudes (elements on $\mathbb{C}/\tilde{\Gamma}$). Let us denote a stochastic Riemannian process (e.g., Gaussian process) on $\mathbb{S}^2$ as $\{p(t)\}_{t\in[0,1]}$, and with associated TSRVC representation (x, q) given by

$$x = p(0), \qquad q(t) = \left(\frac{\dot{p}(t)}{\sqrt{|\dot{p}(t)|}}\right)^{\|}_{p(t)\to p(0)}.$$

4.1 The sample Fréchet mean on $\mathbb{C}$

To estimate the mean of the stochastic Riemannian process, we consider the Fréchet function $F(p_\mu) = \mathbb{E}\left(d^2_{\mathbb{C}}(p, p_\mu)\right)$, and its finite-version

$$F_n(p_\mu; p_1, \ldots, p_n) = \frac{1}{n}\sum_{i=1}^{n} d^2_{\mathbb{C}}(p_i, p_\mu).$$

Then the estimator of the mean is given by the sample Fréchet mean

$$p_\mu = \operatorname*{argmin}_{p\in\mathscr{F}} F_n(p; p_1,\dots,p_n). \tag{11}$$

We now derive computational algorithms to solve (11). We can rewrite the Fréchet function on $\mathbb{C}$ as a function of $x \in \mathbb{S}^2$ and base-curves β_i:

$$\begin{aligned} F_n(x,\beta_1,\dots,\beta_n) =& \frac{1}{n}\sum_{i=1}^{n} d^2_{\beta_i}\Big(\big(x_i, q_i(t)\big), \big(x, q(t,x,\beta_1,\dots,\beta_n)\big)\Big) \\ =& \frac{1}{n}\sum_{i=1}^{n}\Big(\ell^2_{\beta_i} + \int_0^1 |q - q^{||}_{i,\beta_i}|^2 \mathrm{d}t\Big), \end{aligned}$$

where we have

$$q = q(t,x,\beta_1,\dots,\beta_n) = \frac{1}{n}\sum_{i=1}^{n} q^{||}_{i,\beta_i}(t), \tag{12}$$

with $q^{||}_{i,\beta_i}$ being the parallel transportations of $q_i(t)$ along β_i, $q^{||}_{i,\beta_i}(t) = \big(q_i(t)\big)^{||}_{\beta_i(0)\to\beta_i(1)}$. We then optimize F_n iteratively with respect to x and β_i's to obtain the sample Fréchet mean on $\mathbb{C}$:

$$\begin{aligned} \big(\beta^x_1,\dots,\beta^x_n\big) &= \operatorname*{argmin}_{\beta_1,\dots,\beta_n} F_n(x,\beta_1,\dots,\beta_n), \\ x &= \operatorname*{argmin}_{x\in\mathbb{S}^2} F_n\Big(x, q\big(t,x,\beta^x_1,\dots,\beta^x_n\big)\Big). \end{aligned}$$

Therefore the problem of finding the sample Fréchet mean reduces to the optimization problem on the product space $\mathbb{S}^2 \times \big[-\frac{\pi}{2},\frac{\pi}{2}\big]^n$. Since q is determined by the starting point $x \in \mathbb{S}^2$ and the base-curves $\beta_1,\dots,\beta_n$, which are defined by the angles $\theta_1,\dots,\theta_n \in \big[-\frac{\pi}{2},\frac{\pi}{2}\big]$, for a given $x \in \mathbb{S}^2$, we use the gradient descent method to find the optimal

$$\theta = (\theta_1,\dots,\theta_n) = \operatorname*{argmin}_{(\theta_1,\dots,\theta_n)\in\big[-\frac{\pi}{2},\frac{\pi}{2}\big]^n} F_n\big(x,\beta_1(\theta_1),\dots,\beta_n(\theta_n)\big) \quad , \tag{13}$$

where we have to compute

$$\nabla_\theta F_n\big(x,\beta_1(\theta_1),\dots,\beta_n(\theta_n)\big) = \big(\hat{F}_{1n\theta}(p_1,p,\theta_1),\dots,\hat{F}_{nn\theta}(p_n,p,\theta_n)\big),$$

where $\hat{F}_{in\theta}(p_i,p,\theta_i) = \frac{\partial}{\partial\theta_i} d^2(p_i,p,\theta)$. We propose the following Algorithm 3 to find the optimal $\theta = \big(\theta_1,\dots,\theta_n\big)$.

Algorithm 3: The method for finding optimal $\theta = (\theta_1,\dots,\theta_n)$ for (13)

Input: observed functions $p_1,\cdots,p_n$, the point $x \in \mathbb{S}^2$, the initial value $\theta_0 \in \big[-\frac{\pi}{2},\frac{\pi}{2}\big]^n$, the gradient step $\lambda_1 \in \mathbb{R}$, and the degree of accuracy $\varepsilon_1 \in \mathbb{R}$

Output: a vector $\theta = (\theta_1,\dots,\theta_n) \in \big[-\frac{\pi}{2},\frac{\pi}{2}\big]^n$

```
begin
    Set θ = θ_0.
    repeat
        Compute θ̄ = θ − λ_1 ∇_θ F_n(x, β_1(θ_1), ..., β_n(θ_n)).
        if θ̄ ∈ [−π/2, π/2]^n  and  F_n(x, β_1(θ̄_1), ..., β_n(θ̄_n)) < F_n(x, β_1(θ_1), ..., β_n(θ_n)) then
            θ = θ̄;
        else
            λ_1 = λ_1/2;
    until ‖∇_θ F_n(x, θ_1, ..., θ_n)‖ < ε_1;
```

Similarly, for given $\theta = (\theta_1,\cdots,\theta_n)$, we perform the gradient descent algorithm to find the optimal x according to $\operatorname{argmin}_{x\in\mathbb{S}^2} F_n\big(x,\beta_1(\theta_1),\dots,\beta_n(\theta_n)\big)$, where we have to compute

$$\nabla_x F_n\big(x,\beta_1(\theta_1),\dots,\beta_n(\theta_n)\big) = \frac{1}{n}\sum_{i=1}^{n}\nabla_x d^2(p_i,p,\theta_i),$$

Algorithm 4: Sample Fréchet mean calculation on $\mathbb{C}$

Input: the observed functions $p_1, \ldots, p_n$, the gradient steps $\lambda_1, \lambda_2 \in \mathbb{R}$, and the degrees of accuracy $\varepsilon_1, \varepsilon_2 \in \mathbb{R}$

Output: $x_\mu \in \mathbb{S}^2$, $q_\mu \in \mathbb{C}_{x_\mu}$ and the vector $\theta \in \left[-\frac{\pi}{2}, \frac{\pi}{2}\right]^n$.

begin

Set $x = \frac{x_1 + \cdots + x_n}{|x_1 + \cdots + x_n|}$, where $x_i = p_i(0)$.

repeat

Compute θ using Algorithm 3 with input $(p_1, \ldots, p_n, x, \theta, \lambda_1, \varepsilon_1)$.

Set $x = \exp_x\Big(-\lambda_2 \nabla_x F_n\big(x, \beta_1(\theta_1), \ldots, \beta_n(\theta_n)\big)\Big)$, where $\exp_x(\cdot)$ represents the exponential map on $\mathbb{S}^2$.

until $\left|\nabla_x F_n\big(x, \beta_1(\theta_1), \ldots, \beta_n(\theta_n)\big)\right| < \varepsilon_2$;

The explicit expression for $\nabla_x d^2(p_i, p, \theta_i)$ can be found in the supplement. Procedure 4 describes the full algorithm to find the sample Fréchet mean on $\mathbb{C}$.

Remark: since each squared distance function $d^2_{\mathbb{C}}(p_i, \cdot)$ is convex in some neighborhood $U_i \in \mathbb{C}$ of p_i, the Fréchet function should be convex at the intersection of the convex neighborhoods U_i, $U = \bigcap_{i=1}^n U_i$. So if we choose an appropriate initial point $p^0_\mu \in U$, for any gradient descent algorithm, we should converge to the local optimal point p_μ by linear convergence rate.

4.2 The sample Fréchet mean on $\mathbb{C}/\tilde{\Gamma}$

To calculate the mean of functions in $\mathbb{C}/\tilde{\Gamma}$, we have to incorporate the alignment process. Given a set of smooth functions $p_1, \ldots, p_n$, we analyze their amplitudes by choosing an element $\tilde{p}_i$ from each $[p_i]$ and working with $\tilde{p}_1, \ldots, \tilde{p}_n$ using the geometry structure defined for $\mathbb{C}$. Here $\tilde{p}_1, \ldots, \tilde{p}_n$ are well aligned among each other so that $I = \operatorname{argmin}_{\gamma \in \tilde{\Gamma}} d_{\mathbb{C}}(\tilde{p}_i(\gamma), \tilde{p}_j)$ for $i \neq j$ with I being the identity function. Therefore, with an appropriate initialization, we take the following iterative procedure to calculate the Fréchet mean $\tilde{p}_\mu$ and its TSRVC $(\tilde{x}_\mu, \tilde{q}_\mu)$ on $\mathbb{C}/\tilde{\Gamma}$:

1. Update alignment between $\tilde{p}_1, \ldots, \tilde{p}_n$ and $\tilde{p}_\mu$, and update $\tilde{p}_\mu$;
2. Update the base-curves β^*_i between $x_1, \ldots, x_n$ and $\tilde{x}_\mu$
3. Update $\tilde{x}_\mu$

For step 1, we adopt the Procrustes process from [21]. For given $\tilde{x}_\mu \in \mathbb{S}^2$, β^*_i, the $\tilde{q}_\mu$ is first computed as the average of the transported TSRVCs $\tilde{q}_\mu(t) = \frac{1}{n}\sum_{i=1}^n q^{||}_{i,\beta^*_i}(t)$. We then pair-wisely align every transported TSRVC $q^{||}_{i,\beta^*_i}(t)$ to $\tilde{q}_\mu$ with $\gamma_i = \operatorname{argmin}_{\gamma \in \Gamma} d^2_{\beta^*_i}(p_i \circ \gamma, \tilde{p}_\mu)$, and set $\tilde{p}_i = p_i(\gamma_i)$. Next, set $\tilde{q}_\mu(t) = \frac{1}{n}\sum_{i=1}^n \tilde{q}^{||}_{i,\beta^*_i}(t)$, where $\tilde{q}^{||}_{i,\beta^*_i}(t)$ is the transported TSRVC of $\tilde{p}_i$. For steps 2 and 3, we use similar algorithms as the ones presented in section 4.1. Therefore, we develop the following algorithms for computing $\tilde{p}_\mu$.

Algorithm 5 allows us to finish steps 1 and 2. We now integrate results from Algorithm 5 with an algorithm to update x_μ to finalize our computational procedure (presented in Algorithm 6) for calculating the sample mean amplitude.

4.3 Statistical properties of the Fréchet mean

For the Riemannian stochastic process $p = (x, q) \in \mathbb{C}$ we have the Fréchet mean

$$p^* = (x^*, q^*) = \operatorname*{argmin}_{\hat{p} \in \mathbb{C}} \mathbb{E} d^2_{\mathbb{C}}(\hat{p}, p).$$

We can consider the tangent space at $p^* = (x^*, q^*)$ (denoted as $T_{p^*}\mathbb{C}$ for notation simplicity) as a functional space $\mathbb{L}_2([0,1], T_{x^*}\mathbb{S}^2 \times T_{x^*}\mathbb{S}^2)$ with imposed constraints that first functions are constants. The main issue here is that there exists statistical framework for vectors and vector-functions but not for the direct product of a vector space and vector-function space. The difficulty is to determine the covariant function Σ. We consider our space of interest as the principal in the vector-function space and therefore define the covariant function at the vector-function space. We have the following covariant function on $\mathbb{L}_2([0,1], T_{x^*}\mathbb{S}^2 \times T_{x^*}\mathbb{S}^2)$

$$\Sigma = \mathbb{E}\nabla d^2_{\mathbb{C}}(p, p^*) \otimes \nabla d^2_{\mathbb{C}}(p, p^*) = 4\mathbb{E}\exp^{-1}_{p^*} p \otimes \exp^{-1}_{p^*} p,$$

Algorithm 5: The method for finding optimal base-curves $\beta_1^*, \dots, \beta_n^*$ on $\mathbb{C}/\tilde{\Gamma}$

Input: $p_1, \dots, p_n$, the point $\tilde{x}_\mu \in \mathbb{S}^2$, the initial vector $\theta_0 \in \left[-\frac{\pi}{2}, \frac{\pi}{2}\right]^n$, the gradient step $\lambda_1 \in \mathbb{R}$, and the degree of accuracy $\varepsilon_1 \in \mathbb{R}$

Output: a vector $\theta = (\theta_1, \dots, \theta_n)$ for $\beta_1^*, \dots, \beta_n^*$ and aligned paths $\tilde{p}_1, \dots, \tilde{p}_n$

begin

  Set $\tilde{p}_i = p_i = (x_i, q_i)$ for $i = 1, \dots, n$ and $\theta = \theta_0$.

  repeat

    Align $q_1, \dots, q_n$ to $\tilde{q}_\mu = \frac{1}{n}\sum_{i=1}^n q^{||}_{i,\beta_i(\theta_i)}$ at $\mathbb{C}_{x_\mu}$,

    Compute $\bar{\theta} = \theta - \lambda_1 \nabla_\theta F_n\big(x, \beta_1(\theta_1), \dots, \beta_n(\theta_n)\big)$.

    if $\bar{\theta} \in \left[-\frac{\pi}{2}, \frac{\pi}{2}\right]^n$ and $F_n\big(x, \beta_1(\bar{\theta}_1), \dots, \beta_n(\bar{\theta}_n)\big) < F_n\big(x, \beta_1(\theta_1), \dots, \beta_n(\theta_n)\big)$ **then**

      $\theta = \theta - \lambda_1 \nabla_\theta F_n\big(x, \beta_1(\theta_1), \dots, \beta_n(\theta_n)\big)$;

    else

      $\lambda_1 = \frac{\lambda_1}{2}$;

  until $\left|\nabla_\theta F_n(x, \beta_1(\theta_1), \dots, \beta_n(\theta_n))\right| < \varepsilon_1$;

Algorithm 6: Sample Fréchet mean calculation in $\mathbb{C}/\tilde{\Gamma}$

Input: $p_1, \dots, p_n \in \mathbb{C}$, two gradient steps $\lambda_1, \lambda_2 \in \mathbb{R}$, and degrees of accuracy $\varepsilon_1, \varepsilon_2 \in \mathbb{R}_+$

Output: Fréchet mean $\tilde{p}_\mu$ represented as $(\tilde{x}_\mu, \tilde{q}_\mu)$, aligned functions $\tilde{p}_1, \dots, \tilde{p}_n$ to p_μ, and base-curves β_i connecting $x_1, \dots, x_n$ with $\tilde{x}_\mu$ in the form of θ.

begin

  Set $x = \frac{x_1 + \dots + x_n}{|x_1 + \dots + x_n|}$, $\theta = 0$, and $\tilde{p}_i = p_i$ for $i = 1, \dots, n$.

  repeat

    Compute $\theta(x), \tilde{p}_1, \dots, \tilde{p}_n$ from Algorithm 5 with inputs $(p_1, \dots, p_n, x, \theta, \lambda_1, \varepsilon_1)$.

    Set $x = \exp_x\Big(-\lambda_2 \nabla_x \hat{F}_n\big(x, \beta_1(\theta_1), \dots, \beta_n(\theta_n)\big)\Big)$.

  until $\Big|\nabla_x F_n\big(x, \beta_1(\theta_1), \dots, \beta_n(\theta_n)\big)\Big| < \varepsilon_2$;

that maps $(\bar{u}, \bar{w}) \in \mathbb{L}_2([0,1], T_{x^*}\mathbb{S}^2 \times T_{x^*}\mathbb{S}^2)$ with respect to an orthonormal basis for $T_{x^*}\mathbb{S}^2$ as follow

$$\big(\Sigma(\bar{u}, \bar{w})\big)(s) = \big(\hat{u}, \hat{w}(s)\big), \qquad \text{with} \quad \begin{aligned} \begin{pmatrix} \hat{u}^1 \\ \hat{u}^2 \end{pmatrix} &= \begin{pmatrix} \kappa_1^1 & \kappa_2^1 \\ \kappa_1^2 & \kappa_2^2 \end{pmatrix} \begin{pmatrix} \bar{u}^1 \\ \bar{u}^2 \end{pmatrix} + \int_0^1 \begin{pmatrix} k_1^1(t) & k_2^1(t) \\ k_1^2(t) & k_2^2(t) \end{pmatrix} \begin{pmatrix} \bar{w}^1(t) \\ \bar{w}^2(t) \end{pmatrix} \mathrm{d}t, \\ \begin{pmatrix} \hat{w}^1(s) \\ \hat{w}^2(s) \end{pmatrix} &= \begin{pmatrix} k_1^1(s) & k_2^1(s) \\ k_1^2(s) & k_2^2(s) \end{pmatrix} \begin{pmatrix} \bar{u}^1 \\ \bar{u}^2 \end{pmatrix} + \int_0^1 \begin{pmatrix} K_1^1(s,t) & K_2^1(s,t) \\ K_1^2(s,t) & K_2^2(s,t) \end{pmatrix} \begin{pmatrix} \bar{w}^1(t) \\ \bar{w}^2(t) \end{pmatrix} \mathrm{d}t, \end{aligned}$$

for

$$\kappa_j^i = \mathbb{E} u^i u^j, \quad k_j^i(t) = \mathbb{E} u^i w^j(t), \quad K_j^i(s,t) = \mathbb{E} w^i(s) w^j(t).$$

In an Euclidean space, for a sequence of d-dimensional random vectors $X_1, \dots, X_n$ with a finite expectation vector $\mu = \mathbb{E}X$ and covariance Σ, we have

$$\sqrt{n}\left(\frac{1}{n}\sum_{i=1}^n X_i - \mu\right) \to N(0, \Sigma).$$

In a Riemannian manifold, we do not have linearity and instead of $p_\mu - p^*$, we consider $\exp_{p^*}^{-1} p_\mu$, where p_μ is the sample Fréchet mean. For $y = (u, w) \in T_{p^*}\mathbb{C}$ one can take $h_n(y) = F_n(\exp_{p^*} y; p_1, \dots, p_n)$ and get

$$\nabla h_n(y) = \nabla F_n(\exp_{p^*} y; p_1, \dots, p_n) D(\exp_{p^*} y),$$

where $D(\exp_{p^*} y)$ is the differential of the exponential mapping $\exp_{p^*}$ at p^*. Thus since $\nabla F_n(p_\mu; p_1, \dots, p_n) = 0$, we have

$$\nabla h_n(\exp_{p^*}^{-1} p_\mu) = 0.$$

Therefore by the Taylor theorem for some $\delta \in [0,1]$

$$\nabla h_n(0) + \nabla^2 h_n(\delta \exp_{p^*}^{-1} p_\mu) \exp_{p^*}^{-1} p_\mu = 0.$$

Hence for

$$\Lambda = \mathbb{E}\nabla^2 d_{\mathbb{C}}^2(p, p^*)(s,t).$$

we have

$$\sqrt{n} \exp_{p^*}^{-1} p_\mu = -\Lambda^{-1}\left(\frac{1}{\sqrt{n}} \sum_{i=1}^{n} \exp_{p^*}^{-1} p_i\right)$$

Finally, as the generalization of the central limit theorem from [2] we have the following theorem.

Theorem 2. Let $p_1 = p, \ldots, p_n$ be i.i.d. sample. Then

$$\sqrt{n} \exp_{p^*}^{-1} p_\mu \longrightarrow N(0, \Lambda^{-1}\Sigma\Lambda^{-1}).$$

For $\nabla d_{\mathbb{C}}(p_0, p)$ one can look at the supplement.

5 Simulation Studies

In this section, we demonstrate the computational tools we developed using simulated data and compare them with existing ones, e.g. those in [30].

We first simulate curves on $\mathbb{S}^2$ according the following probabilistic model. A mean function p^* is first simulated and then we generate a random covariate function Σ on the tangent space $T_{p^*}\mathbb{C}$. Using a Gaussian process (GP) model

$$(u_i, w_i) \simeq GP\big(0, \Sigma\big), \quad \text{with} \quad \Sigma = \begin{pmatrix} \kappa_1^1 & \kappa_2^1 & k_1^1(t) & k_2^1(t) \\ \kappa_1^2 & \kappa_2^2 & k_1^2(t) & k_2^2(t) \\ k_1^1(s) & k_2^1(s) & K_1^1(s,t) & K_2^1(s,t) \\ k_1^2(s) & k_2^2(s) & K_1^2(t,s) & K_2^2(s,t) \end{pmatrix}. \tag{14}$$

We simulate random tangent vectors (u, w) and map them back to $\mathbb{S}^2$ using the exponential mapping $\exp_{p^*}(\cdot)$. In total, we simulated 8 mean functions p^* with different shapes, and for each p^*, we generated a random covariance function Σ, and sampled 10 functions. Next, for a total of 80 functions, we inserted phase variability to these functions (Figure 12 describes the process of inserting phase variability). For any two functions p_0, p, Algorithm 2 was used to align them and compare their amplitude difference. Figure 9 shows a few examples of geodesics between the amplitudes of a pair of functions. We compared our Algorithm 2 with the one described in [30] (equation (7) in [30]). It is important to note that the algorithm from [30] only computes approximated geodesic distance. More specifically, their parallel transports along the base-curve β are compromised by a numerical approximation procedure. The parallel transport of TSRVC is approximated by many small parallel transports along a piece-wise geodesic approximation of β. Moreover, to find the best β, they use an exhaustive search algorithm. As a consequence, the algorithm from [30] crucially depends on N, the number of discrete points on β, and M, the number of discrete searching points on the range of $[0, 2\pi)$ for finding the optimal β.

From Figure 9 we see that our new algorithm can give better geodesic distances compared with the one in [30]. The improvement is more significant when the shapes of functions compared are more complex (e.g., the second to the fourth rows). For the algorithm in [30], one can observe that when M increases the squared distance decreases, since the chance of finding the best β increases. When N increases the geodesic increases. This is because when N increases, the quality of approximation of β improves and the squared length of the baseline ℓ_β^2 increases (in [30] this values is approximated from below).

We then compared pair-wise differences among the 80 simulated functions, and Figure 10 panel (a) shows pairwise squared distance matrix computed with our Algorithm 2. The same matrix was also computed using the algorithm in [30] with $N = 120$ and $M = 240$. Panel (b) shows the difference matrix between the two algorithms (squared distance of [30] - squared distance of Algorithm 2). Let d_a^2 represent the squared distance from Algorithm 2 and d_b^2 from [30]. We calculate the percentage of improvement of Algorithm 2 based on $100 * (d_b^2 - d_a^2)/d_b^2$, and show a histogram of these percentages in panel (c). We see that the proposed algorithm improves the geodesic calculation in most cases. Actually, the average percentage of improvement is around 9%, indicating that we have significantly improved the geodesic computation.

Next, we consider the sample Fréchet mean on $\mathbb{C}/\tilde{\Gamma}$. Given a set of functions $\{p_1, \ldots, p_n\}$, to optimize the Fréchet function, the proposed Algorithm 6 performs the following steps: 1) for a given starting point $x \in \mathbb{S}^2$, it jointly updates

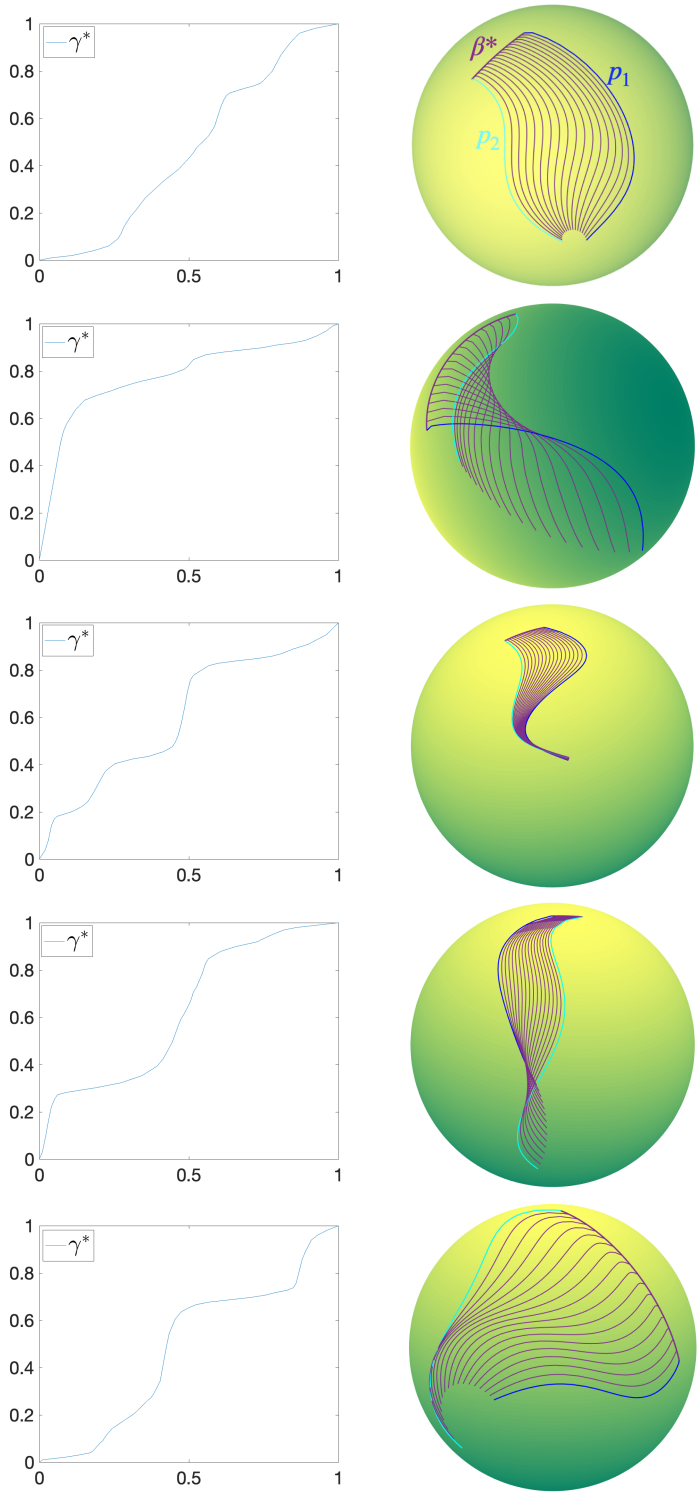

Methods	$d^2_{\mathbb{C}/\Gamma}(p_1, p_2)$
Algorithm 2	0.778398
[30] with $N = 30, M = 60$	0.810474
[30] with $N = 30, M = 120$	0.810315
[30] with $N = 30, M = 240$	0.810237
[30] with $N = 60, M = 60$	0.810529
[30] with $N = 60, M = 120$	0.810369
[30] with $N = 60, M = 240$	0.81029
[30] with $N = 120, M = 60$	0.810542
[30] with $N = 120, M = 120$	0.810382
[30] with $N = 120, M = 240$	0.810304

Methods	$d^2_{\mathbb{C}/\Gamma}(p_1, p_2)$
Algorithm 2	2.52071
[30] with $N = 30, M = 60$	2.56984
[30] with $N = 30, M = 120$	2.56965
[30] with $N = 30, M = 240$	2.56952
[30] with $N = 60, M = 60$	2.57047
[30] with $N = 60, M = 120$	2.57031
[30] with $N = 60, M = 240$	2.57016
[30] with $N = 120, M = 60$	2.57062
[30] with $N = 120, M = 120$	2.57047
[30] with $N = 120, M = 240$	2.57034

Methods	$d^2_{\mathbb{C}/\Gamma}(p_1, p_2)$
Algorithm 2	0.237116
[30] with $N = 30, M = 60$	0.270649
[30] with $N = 30, M = 120$	0.270589
[30] with $N = 30, M = 240$	0.270527
[30] with $N = 60, M = 60$	0.270651
[30] with $N = 60, M = 120$	0.270593
[30] with $N = 60, M = 240$	0.27053
[30] with $N = 120, M = 60$	0.270651
[30] with $N = 120, M = 120$	0.270593
[30] with $N = 120, M = 240$	0.270531

Methods	$d^2_{\mathbb{C}/\Gamma}(p_1, p_2)$
Algorithm 2	0.483469
[30] with $N = 30, M = 60$	0.540953
[30] with $N = 30, M = 120$	0.540949
[30] with $N = 30, M = 240$	0.540947
[30] with $N = 60, M = 60$	0.54096
[30] with $N = 60, M = 120$	0.540956
[30] with $N = 60, M = 240$	0.540955
[30] with $N = 120, M = 60$	0.540962
[30] with $N = 120, M = 120$	0.540958
[30] with $N = 120, M = 240$	0.540956

Methods	$d^2_{\mathbb{C}/\Gamma}(p_1, p_2)$
Algorithm 2	2.63583
[30] with $N = 30, M = 60$	2.64099
[30] with $N = 30, M = 120$	2.63927
[30] with $N = 30, M = 240$	2.6393
[30] with $N = 60, M = 60$	2.64242
[30] with $N = 60, M = 120$	2.64071
[30] with $N = 60, M = 240$	2.64064
[30] with $N = 120, M = 60$	2.64277
[30] with $N = 120, M = 120$	2.64106
[30] with $N = 120, M = 240$	2.64096

(a) (b) (c)

Figure 9: Geodesic calculation between two function amplitudes. Panel (a) shows the warping function γ^* obtained by Algorithm 2, panel (b) shows the two functions on $\mathbb{S}^2$ and the geodesic between them, and panel (c) shows the table of geodesic distances computed by Algorithm 2 and the algorithm from [30] with various N and M.

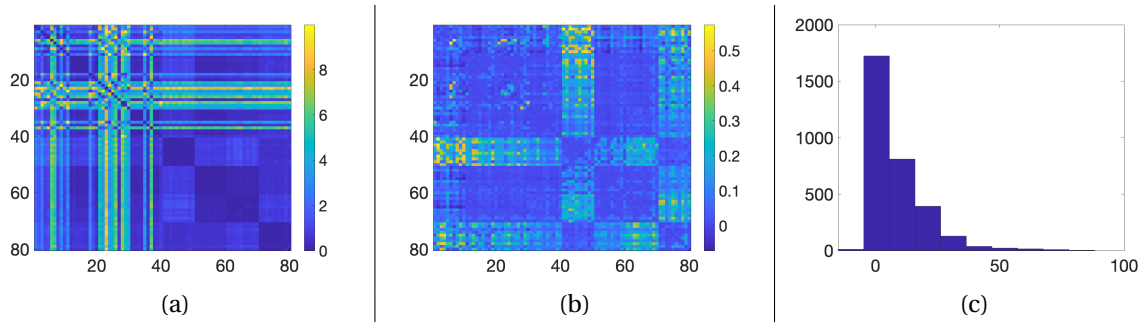

Figure 10: Pairwise squared distance among the amplitudes of 80 simulated functions. Let D_a be the squared distance matrix calculated by Algorithm 2, and D_b be the matrix calculated by the algorithm in [30] (with $N = 120$ and $M = 240$). Panel (a) shows D_a, panel (b) shows $D_b - D_a$, and panel (c) shows the histogram of the upper triangle of $100 * (D_b - D_a)./D_b$.

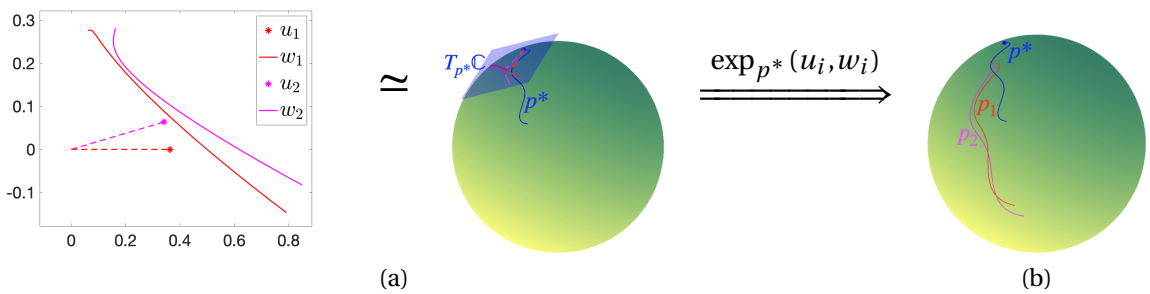

Figure 11: Illustration on data simulation. Panel (a) shows two samples on $T_{p^*}\mathbb{C}$ simulated using the probability model (14). Panel (b) shows two curves $\exp_{p^*}(u_1, w_1)$ and $\exp_{p^*}(u_2, w_2)$ that are interest here.

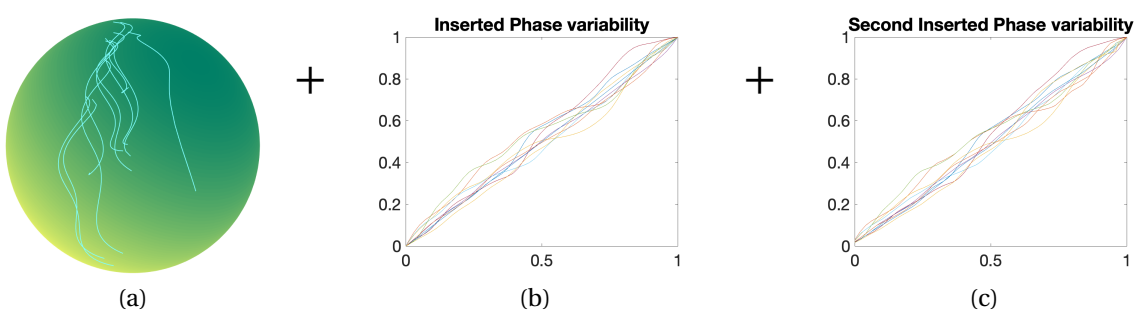

Figure 12: Adding phase variability to simulated functions on $\mathbb{S}^2$. Panel (a) shows curves simulated using the probability model (14). Panel (b) shows the phase variability that was inserted into functions. Panel (c) shows the phase variability that was inserted into functions after inserting the phase variability (b).

the base-curve β_i, the warping function γ_i, and the TSRVC q_μ of the sample Fréchet mean p_μ; and then 2) performs the gradient step using the exponential mapping on $\mathbb{S}^2$, since the gradient of the Fréchet function corresponding to the TSRVC is equal to 0. Similarly, we used a Gaussian process model (14) to simulate tangent vectors on $T_{p^*}\mathbb{C}$ then map it to $\mathbb{C}$ using the exponential mapping $\exp_{p^*}(\cdot)$. Figure 11 panel (a) shows two examples of the sampled (u, w) and panel (b) shows the corresponding functions on $\mathbb{S}^2$. We also inserted phase variability to the simulated functions (see Figure 12). Next, we compared our Algorithm 6 with the one from [30] (Algorithm 3 in [30]) to find the optimal sample Fréchet mean. Figure 13 shows four different examples, where panel (a) shows the phase variability obtained from Algorithm 6, panel (b) shows the simulated functions p_j, the true mean p^*, and the sample mean $\tilde{p}_\mu$, and panel (c) shows the average of mean squared distances obtained from different algorithms. Given the complexity of the simulated functions, apparently, extrinsic mean method, i.e., first calculate the Euclidean mean in $\mathbb{R}^3$ and then map it back to $\mathbb{S}^2$, will not perform well, and hence we did not include in our comparison. From the results, we see that our Fréchet mean captures the amplitude (the shape) of these functions well, and gives a smaller Fréchet function value.

6 Real Data Analysis

We also illustrate our framework on two real datasets: bird migration data [10] and Atlantic hurricane tracks [11] (see Figure 1 for a snapshot of the data).

- The **bird migration data** [10] has 35 migration trajectories of Swainson's Hawk from western North America to Argentina and back, observed from 1995 to 1997. The collected data were used to help identify the most important areas for pesticide control to reduce fatalities of the bird in Argentina.
- The **hurricane data** [11] contains hurricane tracks originated from the Atlantic ocean and Gulf of Mexico. The US National Hurricane Center (NHC) conducted post-storm analyses of hurricanes that have been recorded by the National Oceanic and Atmospheric Administration (NOAA). HURDAT2 is the database we used here and and can be found on `https://www.nhc.noaa.gov/data/`.

We implemented Algorithm 4 to find the sample Fréchet mean of Swainson hawk migrations on $\mathbb{C}$ (see the first row in Figure 14 (a)) and Algorithm 6 to find the sample Fréchet mean on $\mathbb{C}/\Gamma$ (see the first row in Figure 14 (b)). Comparing the two means, we can see that birds travel with non-synchronized speed and the amplitude mean is more representative of the common pattern in the data, e.g., the mean on $\mathbb{C}$ is much shorter than the mean on $\mathbb{C}/\Gamma$ and deviates from the major path due to averaging the non-synchronized trajectories or functions. Similar analysis was also done for the hurricane data and the results are presented in the second row of Figure 14. There is also a descent phase variability in the hurricane data.

To better compare and visualize data on $\mathbb{C}$ and $\mathbb{C}/\Gamma$, we computed the sample covariance matrix of TSRVCs along the sample Fréchet mean before and after alignment. On $T_{p_\mu}\mathbb{C}$ (before alignment), at time t along the mean, we calculate the covariance of the sample TSRVCs as

$$K_\mu(t) = \frac{1}{n-1}\sum_{j=1}^{n} w_j(t) w_j(t)^T \qquad \text{where} \quad (u_j, w_j) = \exp_{p_\mu} p_j,$$

and on $T_{\tilde{p}_\mu}\mathbb{C}/\Gamma$, we have

$$\tilde{K}_\mu(t) = \frac{1}{n-1}\sum_{j=1}^{n} \tilde{w}_j(t) \tilde{w}_j(t)^T \qquad \text{where} \quad (\tilde{u}_j, \tilde{w}_j) = \exp_{\tilde{p}_\mu} \tilde{p}_j.$$

Each $K_\mu(t)$ is a 2×2 tensor and can be plot as an ellipsoid. We parallel transport $K_\mu(t)$ from the tangent space on $T_{p_\mu(0)}\mathbb{S}^2$ to $T_{p_\mu(t)}\mathbb{S}^2$ along p_μ and display them along p_μ. Figure 15 shows these covariance matrices before alignment (panel (a)) and after alignment (panel (c)). We also computed the trace of $K_\mu(t)$ ($\rho_\mu(t) = \text{trace}\big(K_\mu(t)\big)$ and $\tilde{\rho}_\mu(t) = \text{trace}\big(\tilde{K}_\mu(t)\big)$) to summarize the variance as one number at time t, which is displayed on panel (b). These results show the importance of considering phase variability in functional data analysis on $\mathbb{S}^2$.

At last, we compared our Algorithm 6 with the one from [30] (Algorithm 3 in [30]) in Table 1. We can see that proposed framework achieves a significant improvement (around 20%) in the Swainson hawk data, and a slight improvement in the hurricane data (around 3%) when optimizing the Fréchet function.

7 Conclusion

This paper studies functional data on $\mathbb{S}^2$, and provides a method to intrinsically compute the amplitude mean for a set of samples. Functions on $\mathbb{S}^2$ are represented as a pair, consisting of its starting point and a transported square-root

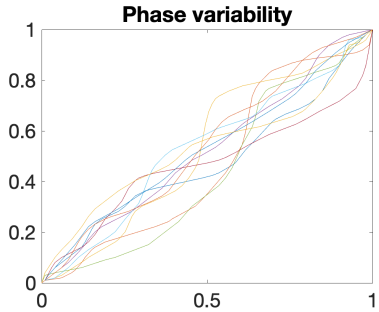

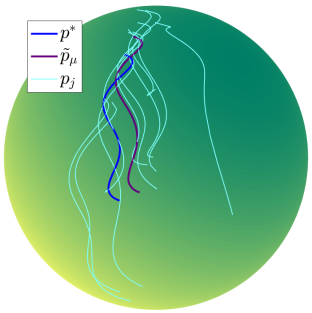

Methods	$\frac{1}{n}\sum_{i=1}^{n} d^2_{\mathbb{C}/\Gamma}(p_i, \tilde{p}_\mu)$
Algorithm 6	0.272878
[30] with $N = 30, M = 60$	0.28613
[30] with $N = 30, M = 120$	0.286135
[30] with $N = 30, M = 240$	0.286153
[30] with $N = 60, M = 60$	0.286137
[30] with $N = 60, M = 120$	0.286144
[30] with $N = 60, M = 240$	0.28616
[30] with $N = 120, M = 60$	0.286139
[30] with $N = 120, M = 120$	0.286146
[30] with $N = 120, M = 240$	0.286162

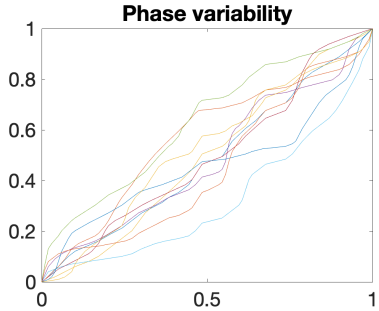

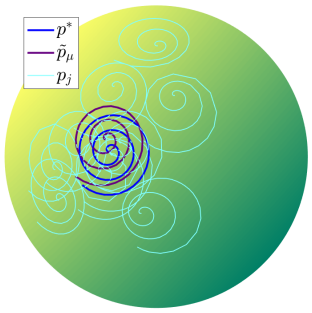

Methods	$\frac{1}{n}\sum_{i=1}^{n} d^2_{\mathbb{C}/\Gamma}(p_i, \tilde{p}_\mu)$
Algorithm 6	0.225475
[30] with $N = 30, M = 60$	0.243124
[30] with $N = 30, M = 120$	0.236718
[30] with $N = 30, M = 240$	0.236772
[30] with $N = 60, M = 60$	0.243322
[30] with $N = 60, M = 120$	0.236672
[30] with $N = 60, M = 240$	0.236792
[30] with $N = 120, M = 60$	0.243327
[30] with $N = 120, M = 120$	0.236677
[30] with $N = 120, M = 240$	0.236797

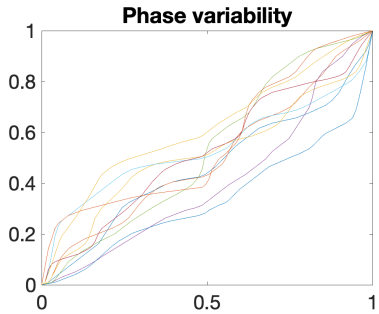

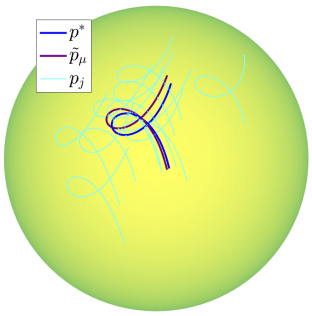

Methods	$\frac{1}{n}\sum_{i=1}^{n} d^2_{\mathbb{C}/\Gamma}(p_i, \tilde{p}_\mu)$
Algorithm 6	0.124914
[30] with $N = 30, M = 60$	0.130731
[30] with $N = 30, M = 120$	0.13071
[30] with $N = 30, M = 240$	0.130721
[30] with $N = 60, M = 60$	0.130741
[30] with $N = 60, M = 120$	0.130719
[30] with $N = 60, M = 240$	0.130731
[30] with $N = 120, M = 60$	0.130743
[30] with $N = 120, M = 120$	0.130721
[30] with $N = 120, M = 240$	0.130733

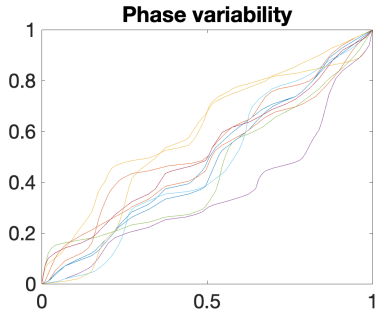

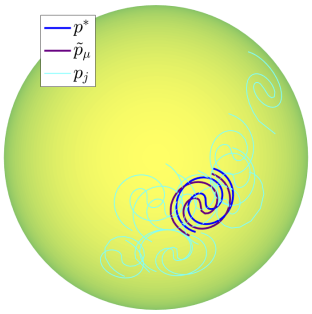

Methods	$\frac{1}{n}\sum_{i=1}^{n} d^2_{\mathbb{C}/\Gamma}(p_i, \tilde{p}_\mu)$
Algorithm 6	0.217113
[30] with $N = 30, M = 60$	0.231254
[30] with $N = 30, M = 120$	0.23092
[30] with $N = 30, M = 240$	0.230834
[30] with $N = 60, M = 60$	0.231281
[30] with $N = 60, M = 120$	0.230947
[30] with $N = 60, M = 240$	0.230861
[30] with $N = 120, M = 60$	0.231288
[30] with $N = 120, M = 120$	0.230953
[30] with $N = 120, M = 240$	0.230868

(a) (b) (c)

Figure 13: Examples of sample Fréchet mean for function amplitudes. Panel (a) shows the warping function $\{\gamma_1, \ldots, \gamma_n\}$ obtained by Algorithm 6, panel (b) shows the sample data $\{p_1, \ldots, p_n\}$, the Fréchet mean p^*, the sample Fréchet mean p_μ, and panel (c) shows a table of optimal sample Féchet functions computed by Algorithm 6 and the algorithm from [30] with various N and M.

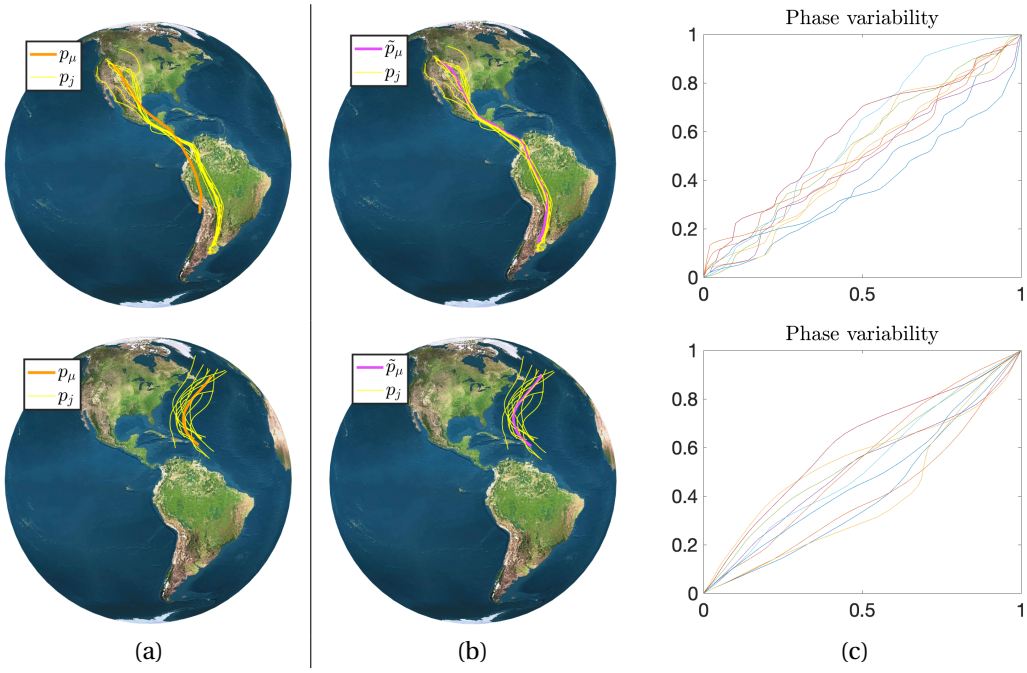

Figure 14: Real data analysis on bird migration trajectories and hurricane paths. Panel (a) shows the sample Fréchet mean p_μ obtained by Algorithm 4. Panel (b) shows the sample Fréchet mean $\tilde{p}_\mu$ derived by Algorithm 6 and the corresponding time warping functions for alignment.

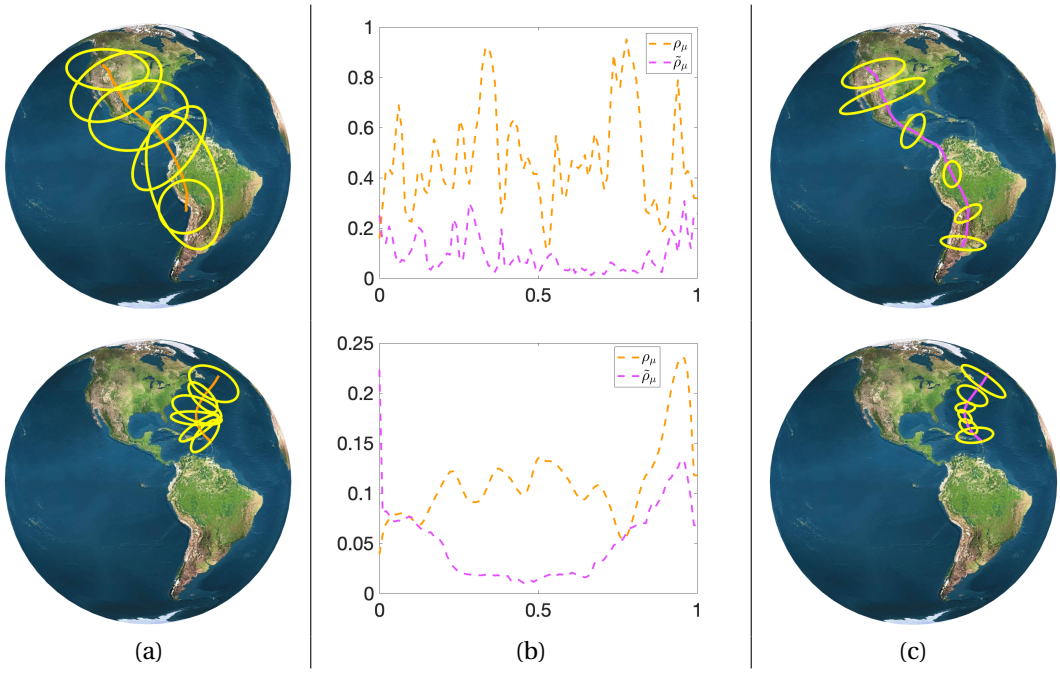

Figure 15: Visualization of variability of TSRVCs before and after alignment. Panel (a) shows the covariance ($K_\mu(t)$) of TSRVCs before alignment, and panel (c) shows the covariance after alignment. Panel (b) shows the trace of $K_\mu(t)$s.

Table 1: Comparison of the Algorithm 6 with the one from [30] to find the sample Fréchet mean on real data.

Swainson hawk data		Hurricane data	
Methods	$\frac{1}{n}\sum_{i=1}^{n} d^2_{\mathbb{C}/\Gamma}(p_i, \tilde{p}_\mu)$	Methods	$\frac{1}{n}\sum_{i=1}^{n} d^2_{\mathbb{C}/\Gamma}(p_i, \tilde{p}_\mu)$
Algorithm 6	0.105873	Algorithm 6	0.052998
[30] with $N = 30, M = 60$	0.136115	[30] with $N = 30, M = 60$	0.0545199
[30] with $N = 30, M = 120$	0.136112	[30] with $N = 30, M = 120$	0.0545143
[30] with $N = 30, M = 240$	0.136113	[30] with $N = 30, M = 240$	0.0545157
[30] with $N = 60, M = 60$	0.136115	[30] with $N = 60, M = 60$	0.0545207
[30] with $N = 60, M = 120$	0.136112	[30] with $N = 60, M = 120$	0.0545143
[30] with $N = 60, M = 240$	0.136113	[30] with $N = 60, M = 240$	0.0545158
[30] with $N = 120, M = 60$	0.136116	[30] with $N = 120, M = 60$	0.0545207
[30] with $N = 120, M = 120$	0.136112	[30] with $N = 120, M = 120$	0.0545143
[30] with $N = 120, M = 240$	0.136113	[30] with $N = 120, M = 240$	0.0545158

curve (TSRVC). With this representation, the domain of interest becomes a fiber bundle, denoted as $\mathbb{C}$. We then study the Riemannian structure of $\mathbb{C}$, and its quotient space $\mathbb{C}/\tilde{\Gamma}$ containing the amplitude of smooth functions. Gradient descent algorithms are developed to find the geodesic between two points on $\mathbb{C}$ and $\mathbb{C}/\tilde{\Gamma}$. In this process, we simplify the geodesic search by developing several novel tools, including closed form solutions for parallel transport of vectors along circle arcs on $\mathbb{S}^2$, and a closed form gradient of the distance function between two functions. From there, we extend our toolbox to perform analysis of a set of functions and by developing computational algorithms for finding the sample Fréchet means on $\mathbb{C}$ and $\mathbb{C}/\tilde{\Gamma}$, where novel exponential and inverse exponential maps are introduced. The proposed framework is comprehensively evaluated in both simulated and real data, and is shown to be superior to its competitor. Implementation of these tools is published on GitHub repository: `https://github.com/Bayan2019/2DSphericalTrajectories`.

References

[1] Bertsekas, D. P. (1995). *Dynamic Programming and Optimal Control* (1st ed.). Athena Scientific.

[2] Bhattacharya, A. and R. Bhattacharya (2012). *Nonparametric Inference on Manifolds: With Applications to Shape Spaces*. Institute of Mathematical Statistics Monographs.

[3] Bowman, A. (2010). Functional data analysis with R and MATLAB. *Journal of Statistical Software 34*(1), 1–2.

[4] Brigant, A. L. (2017). Computing distances and geodesics between manifold-valued curves in the srv framework. *Journal of Geometric Mechanics 9*(2), 131–156.

[5] Ferraty, F. and P. Vieu (2006). *Nonparametric Functional Data Analysis: Methods, Theory, Applications and Implementations*. Springer.

[6] Gervini, D. and T. Gasser (2004). Self-modelling warping functions. *Journal of the Royal Statistical Society: Series B (Statistical Methodology) 66*(4), 959–971.

[7] Hsing, T. and R. Eubank (2015). *Theoretical Foundations of Functional Data Analysis, with an Introduction to Linear Operators*. Wiley Series in Probability and Statistics. Wiley.

[8] James, G. M. (2007, 12). Curve alignment by moments. *The Annals of Applied Statistics 1*(2), 480–501.

[9] Kneip, A. and T. Gasser (1992, 09). Statistical tools to analyze data representing a sample of curves. *20*(3), 1266–1305.

[10] Kochert, M. N., M. R. Fuller, L. S. Schueck, L. Bond, M. J. Bechard, B. Woodbridge, G. L. Holroyd, M. S. Martell, and U. Banasch (2011, 02). Migration Patterns, use of Stopover Areas, and Austral Summer Movements of Swainson's Hawks. *The Condor 113*(1), 89–106.

[11] Landsea, C. and J. Franklin (2013). Atlantic hurricane database uncertainty and presentation of a new database format. *Monthly Weather Review 141*, 3576–3592.

[12] Le Brigant, A. (2019). A discrete framework to find the optimal matching between manifold-valued curves. *Journal of Mathematical Imaging and Vision 61*(1), 40–70.

[13] Lin, Z. and F. Yao (2019, 12). Intrinsic Riemannian functional data analysis. *The Annals of Statistics 47*(6), 3533–3577.

[14] Liu, X. and H.-G. Müller (2004). Functional convex averaging and synchronization for time-warped random curves. *Journal of the American Statistical Association 99*(467), 687–699.

[15] Marron, J. S., J. O. Ramsay, L. M. Sangalli, and A. Srivastava (2014). Statistics of time warpings and phase variations. *Electronic Journal of Statistics 8*(2), 1697–1702.

[16] Michor, P. and D. Mumford (2003). Riemannian geometries on spaces of plane curves. *Journal of the European Mathematical Society 8*, 1–48.

[17] Michor, P. W. and D. Mumford (2007). An overview of the Riemannian metrics on spaces of curves using the Hamiltonian approach. *Applied and Computational Harmonic Analysis 23*(1), 74–113. Special Issue on Mathematical Imaging.

[18] Michor, P. W. and D. K. Mumford (2005). Vanishing geodesic distance on spaces of submanifolds and diffeomorphisms. *Documenta Mathematica 10*, 217–245.

[19] Müller, H.-G. and U. Stadtmüller (2005, 04). Generalized functional linear models. *The Annals of Statistics 33*(2), 774–805.

[20] Ramsay, J. O. and C. J. Dalzell (1991). Some tools for functional data analysis. *Journal of the Royal Statistical Society. Series B (Methodological) 53*(3), 539–572.

[21] Ramsay, J. O. and X. Li (1998). Curve registration. *Journal of the Royal Statistical Society: Series B (Statistical Methodology) 60*(2), 351–363.

[22] Ramsay, J. O. and B. W. Silverman (2005). *Functional Data Analysis*. Springer-Verlag New York.

[23] Ramsay, J. O. and B. W. Silverman (2007). *Applied Functional Data Analysis: Methods and Case Studies*. Springer-Verlag New York.

[24] Sakoe, H. and S. Chiba (1978). Dynamic programming algorithm optimization for spoken word recognition. *IEEE TRANSACTIONS ON ACOUSTICS, SPEECH, AND SIGNAL PROCESSING 26*, 43–49.

[25] Srivastava, A., E. Klassen, S. H. Joshi, and I. H. Jermyn (2011, jul). Shape analysis of elastic curves in Euclidean spaces. *IEEE Transactions on Pattern Analysis and Machine Intelligence 33*(7), 1415–1428.

[26] Su, J., S. Kurtek, E. Klassen, and A. Srivastava (2014, 03). Statistical analysis of trajectories on Riemannian manifolds: Bird migration, hurricane tracking and video surveillance. *The Annals of Applied Statistics 8*(1), 530–552.

[27] Sundaramoorthi, G., A. Yezzi, and A. Mennucci (2005). Sobolev active contours. *International Journal of Computer Vision 73*, 109–120.

[28] Wang, K. and T. Gasser (1997). Alignment of curves by dynamic time warping. *The Annals of Statistics 25*(3), 1251–1276.

[29] Younes, L. (1998). Computable elastic distances between shapes. *SIAM Journal of Applied Mathematics 58*, 565–586.

[30] Zhang, Z., E. Klassen, and A. Srivastava (2018). Phase-amplitude separation and modeling of spherical trajectories. *Journal of Computational and Graphical Statistics 27*(1), 85–97.

[31] Zhang, Z., J. Su, E. Klassen, H. Le, and A. Srivastava (2018). Rate-invariant analysis of covariance trajectories. *Journal of Mathematical Imaging and Vision 60*(8), 1306–1323.

A Supplementary material to "Amplitude Mean of Functional Data on $\mathbb{S}^2$"

A.1 Proof of Theorem 1

Let $e_1,\dots,e_d \in T_{x_0}\mathscr{M}$ be the orthonormal basis on $T_{x_0}\mathscr{M}$. Then one can take their images $e_1^{\|},\dots,e_d^{\|} \in T_x\mathscr{M}$ as basis on $T_x\mathscr{M}$ with

$$e_i^{\|} = \mathscr{P}(\beta)_0^1 e_i, \qquad i = 1,\dots,d,$$

where $\mathscr{P}(\beta)_s^t$ is the parallel transport along β from $\beta(s)$ to $\beta(t)$. Since for any $v \in T_{x_0}\mathscr{M}$

$$\frac{d}{dt}\left\langle \mathscr{P}(\beta)_0^t v, \mathscr{P}(\beta)_0^t e_k \right\rangle = \left\langle \nabla_{\dot\beta}\mathscr{P}(\beta)_0^t v, \mathscr{P}(\beta)_0^t e_k \right\rangle + \left\langle \mathscr{P}(\beta)_0^t v, \nabla_{\dot\beta}\mathscr{P}(\beta)_0^t e_k \right\rangle = 0,$$

so

$$\left\langle \mathscr{P}(\beta)_0^1 v, e_k^{\|} \right\rangle = \langle v, e_k \rangle,$$

then one has

$$\mathscr{P}(\beta)_0^1 v = \sum_{k=1}^d \left\langle \mathscr{P}(\beta)_0^1 v, e_k^{\|} \right\rangle e_k^{\|} = \sum_{k=1}^d \langle v, e_k \rangle e_k^{\|}$$

Therefore one gets

$$\begin{aligned} d_\beta^2\Big(\big(x_0, q_0(\gamma(t))\sqrt{\dot\gamma(t)}\big), \big(x, q(\gamma(t))\sqrt{\dot\gamma(t)}\big)\Big) &= \ell_\beta + \int_0^1 |q_{0,\beta(1)}^{\|}(\gamma(t)) - q(\gamma(t))|^2 \dot\gamma(t)\mathrm{d}t = \\ &= \ell_\beta + \int_0^1 |q_{0,\beta(1)}^{\|}(\gamma(t)) - q(\gamma(t))|^2 \mathrm{d}(\gamma(t)) = \\ &= \ell_\beta + \int_0^1 |q_{0,\beta(1)}^{\|}(t) - q(t)|^2 \mathrm{d}t. \end{aligned}$$

A.2 Parallel transport along the p-optimal curve β on $\mathbb{S}^2$

In figure 1, for any two points $x_0, x \in S^2$, we have a p-optimal curve β, which belongs to the intersection of the sphere $\mathbb{S}^2$ with π_β plane, and the geodesic β_0, which belongs to the intersection of the sphere with π_{β_0} that contains the center of the sphere.

The plane π_β is determined by its normal vector n (an vector orthogonal to π_β). We parameterize n using $\theta \in [-\frac{\pi}{2}, \frac{\pi}{2}]$, measuring the angle between n and the cross product of x_0 and x (i.e., $x_0 \times x$, which is orthogonal to both x_0 and x with a direction given by the right-hand rule and a magnitude equal to the area of the parallelogram that the vectors x_0, x span). Hence one has the following expression for n

$$n(\theta; x_0, x) = \frac{x_0 + x}{|x_0 + x|}\sin\theta + \frac{x_0 \times x}{|x_0 \times x|}\cos\theta. \tag{15}$$

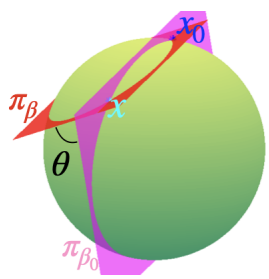

Figure 16: The plane π_β contains β and the plane π_{β_0}, contains β_0 and the center of $\mathbb{S}^2$.

Therefore the p-optimal β curve have the following expressions:

$$\beta(s;\theta) = x_0\cos(s\phi) + (n \times x_0)\sin(s\phi) + n\langle n, x_0\rangle\big(1 - \cos(s\phi)\big),$$

where $\phi = 2\arcsin\left(\frac{1}{2}\sqrt{\frac{2-2\langle x_0,x\rangle}{1-\langle n,x_0\rangle^2}}\right)$.

The p-optimal curve connecting x_0 and x is determined by the angle θ and the path determined by β on $\mathbb{C}$ has the length

$$d(p_0, p, \theta) = d_{\beta(\theta)}(p_0, p) = \sqrt{\ell_{\beta(\theta)}^2 + \int_0^1 \left|q_{0,\beta(\theta)}^{\|}(t) - q(t)\right|^2 \mathrm{d}t}. \tag{16}$$

Hence we have the geodesic distance

$$d_{\mathbb{C}}(p_0, p) = \min_{\theta\in[-\frac{\pi}{2},\frac{\pi}{2}]} \sqrt{\ell_{\beta(\theta)}^2 + \int_0^1 \left|q_{0,\beta(\theta)}^{\|}(t) - q(t)\right|^2 \mathrm{d}t}. \tag{17}$$

On the sphere $\mathbb{S}^2$ we have the following covariant derivative along the curve β

$$\nabla_{\dot\beta} v = \frac{\partial v}{\partial s} - \left\langle \beta, \frac{\partial v}{\partial s} \right\rangle \beta.$$

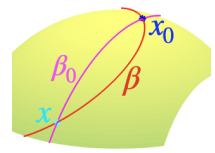

Figure 17: The p-optimal base-curve β and the geodesic β_0 connecting x_0 and x.

Let us consider a parallel tangent vector field $v(s) = \left(v^1(s), v^2(s), v^3(s)\right) \in T_{\beta(s)}\mathbb{S}^2$ along the base-curve $\beta(s)$ with respect to an orthonormal system

$$e_1 = \frac{n \times x_0}{|n \times x_0|} \times n, \qquad e_2 = \frac{n \times x_0}{|n \times x_0|}, \qquad e_3 = n.$$

Under this orthonormal system, the base-curve β has the following expression

$$\beta(s;\theta) = \left(\cos(s\phi)\sin\alpha, \quad \sin(s\phi)\sin\alpha, \quad \cos\alpha\right), \tag{18}$$

where α is the angle between n and x_0. One can obtain

$$\alpha(\theta, x_0, x) = \arccos\left(\sqrt{\frac{1+\langle x_0, x\rangle}{2}}\sin\theta\right)$$

and

$$\phi(\theta, x_0, x) = 2\arcsin\left(\sqrt{\frac{1-\langle x_0, x\rangle}{1+\cos^2\theta - \langle x_0, x\rangle\sin^2\theta}}\right).$$

Proposition 2. The parallel transport of $e_2 \in T_{x_0}\mathbb{S}^2$ along β has the following expression

$$v(\theta, s) = e^{||}_{2,\beta(\theta,s)} = v^1(\theta, s)e_1 + v^2(\theta, s)e_2 + v^3(\theta, s)n,$$

with

$$\begin{aligned}
v^1(\theta, s) &= v^1(s, \alpha, \phi) = \cos(s\phi)\sin(s\phi\cos\alpha)\cos\alpha - \sin(s\phi)\cos(s\phi\cos\alpha),\\
v^2(\theta, s) &= v^2(s, \alpha, \phi) = \cos(s\phi)\cos(s\phi\cos\alpha) + \sin(s\phi)\sin(s\phi\cos\alpha)\cos\alpha,\\
v^3(\theta, s) &= v^3(s, \alpha, \phi) = -\sin(s\phi\cos\alpha)\sin\alpha.
\end{aligned}$$

Proof. In the orthonormal system e_1, e_2, n we have

$$n = \begin{pmatrix} 0\\ 0\\ 1\end{pmatrix}, \quad x_0 = \begin{pmatrix} \sin\alpha\\ 0\\ \cos\alpha\end{pmatrix}, \quad x = \begin{pmatrix} \cos\phi\sin\alpha\\ \sin\phi\sin\alpha\\ \cos\alpha\end{pmatrix}.$$

Since v is the tangent vector field, there

$$\langle \beta, v\rangle = 0,$$

thus

$$v^1(s, x_0, x, \theta, v^2, v^3) = -\frac{v^2\sin(s\phi)\sin\alpha + v^3\cos\alpha}{\cos(s\phi)\sin\alpha}.$$

Also with the help of the equality

$$\langle v, v\rangle = \langle v(0), v(0)\rangle = |e_2|^2 = 1,$$

one finds

$$v^2\left(s, v^3, \alpha, \phi\right) = \frac{\cos(s\phi)\sqrt{\sin^2\alpha - \left(v^3\right)^2} - v^3\sin(s\phi)\cos\alpha}{\sin\alpha}.$$

Then from the fact that v is the parallel tangent vector field one has

$$\nabla_{\dot\beta} v = \frac{\partial v}{\partial s} - \left\langle \beta, \frac{\partial v}{\partial s}\right\rangle \beta = 0.$$

So

$$\dot v = \beta\langle \beta, \dot v\rangle = -\beta\langle \dot\beta, v\rangle. \tag{19}$$

Consequently, this equation comes down to to the differential equation on v^3

$$\dot v^3 = -\phi\cos\alpha\sqrt{\sin^2\alpha - v^3}.$$

Finally from $v(0) = e_2 = (0,1,0)^T$ one gets

$$v(\theta, s) = v(s, x_0, x, \theta) = \begin{pmatrix} v^1 \\ v^2 \\ v^3 \end{pmatrix} = \begin{pmatrix} 0 \\ 1 \\ 0 \end{pmatrix}^{||}_{\beta},$$

where

$$\begin{aligned} v^1(s,\alpha,\phi) &= \cos(s\phi)\sin(s\phi\cos\alpha)\cos\alpha - \sin(s\phi)\cos(s\phi\cos\alpha), \\ v^2(s,\alpha,\phi) &= \cos(s\phi)\cos(s\phi\cos\alpha) + \sin(s\phi)\sin(s\phi\cos\alpha)\cos\alpha, \\ v^3(s,\alpha,\phi) &= -\sin(s\phi\cos\alpha)\sin\alpha. \end{aligned}$$

□

Proposition 3. Let $e^{||}_{2,\beta(\theta,s)} = v(\theta, s)$. Then for any $u \in T_{x_0}\mathbb{S}^2$

$$u^{||}_{\beta(s)} = \langle e_2, u\rangle v(\theta, s) + \langle (e_2 \times x_0), u\rangle \big(v(\theta, s) \times \beta(\theta, s)\big).$$

Proof. The parallel transport map $\mathscr{P}_{\beta(\theta)} : T_{x_0}\mathbb{S}^2 \to T_x\mathbb{S}^2$ can be expressed as a rotation $\mathscr{R}(\theta, s)$

$$\begin{aligned} v(\theta, s) &= \mathscr{R}(\theta, s)e_2, \\ v(\theta, s) \times \beta(\theta, s) &= \mathscr{R}(\theta, s)\big(e_2 \times x_0\big), \\ \beta(\theta, s) &= \mathscr{R}(\theta, s)x_0. \end{aligned}$$

Therefor for any $u = u^1 e_2 + u^2\big(e_2 \times x_0\big) \in T_{x_0}\mathbb{S}^2$ one has

$$\mathscr{R}(\theta, s)u = u^1\mathscr{R}(\theta, s)e_2 + u^2\mathscr{R}(\theta, s)\big(e_2 \times x_0\big)$$

□

So one gets $e^{||}_{2,\beta(\theta,s)} = v(\theta, s)$ and therefore

$$\begin{aligned} q^{||}_{0,\beta(\theta,s)}(t) = q^{||}_s\big(q_0(t), x_0, x, \theta\big) =& \big\langle v(0), q_0(t)\big\rangle v(\theta, s) + \Big\langle \big(v(0) \times x0\big), q_0(t)\Big\rangle \big(v(\theta, s) \times x\big) \\ =& \big\langle e_2, q_0(t)\big\rangle v(\theta, s) + \Big\langle \big(e_2 \times x_0\big), q_0(t)\Big\rangle \big(v(\theta, s) \times x\big). \end{aligned}$$

Thus one gets

$$\begin{aligned} d^2(p_0, p, \theta) = d^2_{\beta(\theta)}(p_0, p) &= \ell^2_{\beta(\theta)} + \int_0^1 \left|q^{||}_{0,\beta(\theta)}(t) - q(t)\right|^2 \mathrm{d}t \\ &= 2\arcsin^2\left(\sqrt{\frac{1 - \langle x_0, x\rangle}{1 + \cos^2\theta - \langle x_0, x\rangle\sin^2\theta}}\right)(1 + \cos^2\theta - \langle x_0, x\rangle\sin^2\theta) \\ &\quad + \int_0^1 \left(\big(\langle e_2, q_0(t)\rangle - \langle v, q(t)\rangle\big)^2 + \Big(\big\langle (e_2 \times x_0), q_0(t)\big\rangle - \langle (v \times x), q(t)\rangle\Big)^2\right)\mathrm{d}t, \end{aligned}$$

where $v = v(1)$. One is interested in

$$\theta(p_0, p) = \underset{\theta \in \left[-\frac{\pi}{2}, \frac{\pi}{2}\right]}{\operatorname{argmin}} d^2(p_0, p, \theta),$$

and one can perform the gradient descent algorithm to find $\theta(p_0, p)$.

A.3 The derivative of $d^2(p_0, p, \theta)$ with respect to θ

One can see that the distance function $d(p_0, p, \theta)$ depends on θ that determines the base-curve β. One can also obtain

$$\begin{aligned} \frac{\partial}{\partial\theta} d^2(p_0, p, \theta) =& 2\phi\sin\alpha\left(\frac{\partial\phi}{\partial\theta}\sin\alpha + \phi\cos\alpha\frac{\partial\alpha}{\partial\theta}\right) \\ &+ \int_0^1 2\left\langle \frac{\partial}{\partial\theta} q^{||}_{0,\beta(1)},\ q^{||}_{0,\beta(1)}(t) - q(t)\right\rangle \mathrm{d}t, \end{aligned}$$

where

$$\frac{\partial}{\partial\theta} q^{||}_{0,\beta(1)} = \left\langle \frac{\partial e_2}{\partial\theta}, q_0(t) \right\rangle v + \left\langle \left(\frac{\partial e_2}{\partial\theta} \times x_0 \right), q_0(t) \right\rangle (v \times x) + \langle e_2, q_0(t)\rangle \frac{\partial v}{\partial\theta} + \langle (e_2 \times x_0), q_0(t)\rangle \left(\frac{\partial v}{\partial\theta} \times x \right),$$

for

$$\frac{\partial v}{\partial\theta} = \frac{\partial v^1}{\partial\theta} e_1 + v^1 \frac{\partial e_1}{\partial\theta} + \frac{\partial v^2}{\partial\theta} e_2 + v^2 \frac{\partial e_2}{\partial\theta} + \frac{\partial v^3}{\partial\theta} n + v^3 \frac{\partial n}{\partial},$$

with

$$\frac{\partial v^1}{\partial\theta} = \frac{\partial v^1}{\partial\alpha}\frac{\partial\alpha}{\partial\theta} + \frac{\partial v^1}{\partial\phi}\frac{\partial\phi}{\partial\theta}, \qquad \frac{\partial v^2}{\partial\theta} = \frac{\partial v^2}{\partial\alpha}\frac{\partial\alpha}{\partial\theta} + \frac{\partial v^2}{\partial\phi}\frac{\partial\phi}{\partial\theta}, \qquad \frac{\partial v^3}{\partial\theta} = \frac{\partial v^3}{\partial\alpha}\frac{\partial\alpha}{\partial\theta} + \frac{\partial v^3}{\partial\phi}\frac{\partial\phi}{\partial\theta},$$

$$\frac{\partial\alpha}{\partial\theta} = -\sqrt{\frac{1+\langle x_0, x\rangle}{1+\cos^2\theta - \langle x_0, x\rangle \sin^2\theta}} \cos\theta, \qquad \frac{\partial\phi}{\partial\theta} = \frac{2\sin(\theta)\sqrt{1-\langle x_0, x\rangle^2}}{1+\cos^2\theta - \langle x_0, x\rangle \sin^2\theta},$$

and

$$D_\theta n = \frac{\partial}{\partial\theta} n(x_0, x, \theta) = \frac{(x_0 + x)\cos\theta}{|x_0 + x|} - \frac{(x_0 \times x)\sin\theta}{|x_0 \times x|},$$

$$\frac{\partial e_2}{\partial\theta} = -\frac{\langle D_\theta n \times x_0, n \times x_0\rangle}{|n \times x_0|^3}(n \times x_0) + \frac{D_\theta n \times x_0}{|n \times x_0|},$$

$$\frac{\partial e_1}{\partial\theta} = -\frac{\langle D_\theta n \times x_0, n \times x_0\rangle}{|n \times x_0|^3}(n \times x_0) \times n + \frac{D_\theta n \times x_0}{|n \times x_0|} \times n + \frac{n \times x_0}{|n \times x_0|} \times D_\theta n.$$

A.4 The exponential and inverse exponential maps on $\mathbb{C}$

For statistical analysis of a set of observations on $\mathbb{C}$, another two important tools are the exponential and inverse exponential maps. Let $(u, w) \in T_{(x,q)}\mathbb{C}$, the exponential map $\exp_{(x,q)}(s(u, w))$ is a mapping from $T_{(x,q)}\mathbb{C}$ to $\mathbb{C}$, and gives a geodesic $(\beta(s), q(s, t))$ on $\mathbb{C}$, where $s \in [0, 1]$. Given two functions or trajectories p_0 and p on $\mathbb{S}^2$, and their TSRVC representations (x_0, q_0) and (x, q), the inverse exponential map $\exp^{-1}_{(x_0,q_0)}(x, q)$ gives a tangent vector (u, w) on $T_{(x_0,q_0)}\mathbb{C}$, such that $\exp_{(x_0,q_0)}((u, w)) = (x, q)$. Since we consider p and (x, q) as the same, for notation simplicity $\exp_p(s(u, w))$ is also used to denote the exponential map from $T_p\mathbb{C}$ to $\mathbb{C}$ and $\exp^{-1}_{p_0} p$ to denote for the inverse exponential map from $\mathbb{C}$ to $T_{p_0}\mathbb{C}$.

On $\mathbb{C}$, once we find the optimal geodesic $\theta \in \left[-\frac{\pi}{2}, \frac{\pi}{2}\right]$ for p_0 and p, it is straightforward to get the inverse exponential map

$$\exp^{-1}_{p_0} p = \left(\dot\beta(0;\theta), q^{||}_\beta - q_0\right),$$

where β is determined by θ. Figure 18 shows one example of p_0 and p on $\mathbb{S}^2$ and the inverse exponential map $\exp^{-1}_{p_0} p$.

The exponential mapping $\exp_{p_0}((u, w))$ is harder to compute than the inverse exponential map. Let $(\beta(s), q(s, \cdot)) = \exp_{p_0}(s(u, w))$ for $s \in [0, 1]$. We need to construct a $(\beta(s), q(s, \cdot))$ that satisfies the two properties in Proposition 1 and $\dot\beta(0) = u$. We describe our procedure to construct such $(\beta(s), q(s, \cdot))$ as follows.

For a given $u \in T_{x_0}\mathbb{S}^2$, we can construct a set of p-optimal curves determined by a set of planes π_β that intersect with $T_{x_0}\mathbb{S}^2$ by the line $x_0 + tu$ for $t \in \mathbb{R}$, where π_β is determined by a normal vector

$$n(\vartheta; x_0, u) = x_0 \cos\vartheta + \frac{x_0 \times u}{|x_0 \times u|}\sin\vartheta \qquad \text{for} \quad \vartheta \in \left(\arcsin\left(\frac{|u|}{\pi}\right), \pi - \arcsin\left(\frac{|u|}{\pi}\right)\right). \tag{20}$$

One can find out that

$$\beta(s;\vartheta) = x_0\cos(s\phi) + (n \times x_0)\sin(s\phi) + n\langle n, x_0\rangle\left(1 - \cos(s\phi)\right) \qquad \text{with} \quad \phi(\vartheta) = \frac{|u|}{\sin\vartheta},$$

$$q(s, t) = \left(s w(t) + q_0(t)\right)^{||}_{\beta(s)}.$$

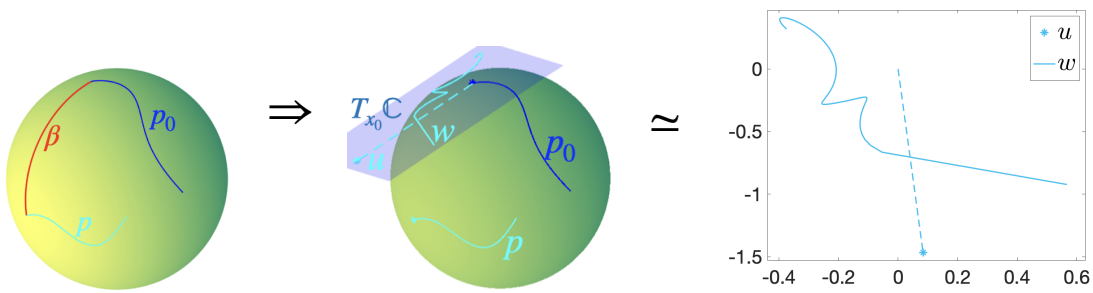

(a) (b)

Figure 18: Panel (a) shows the base-curve β which determines the geodesics on $\mathbb{C}$ between two functions p_0 and p,. Panel (b) shows $(u, w) = \exp_{p_0}^{-1} p$ on the tangent space $T_{x_0}\mathbb{S}^2$.

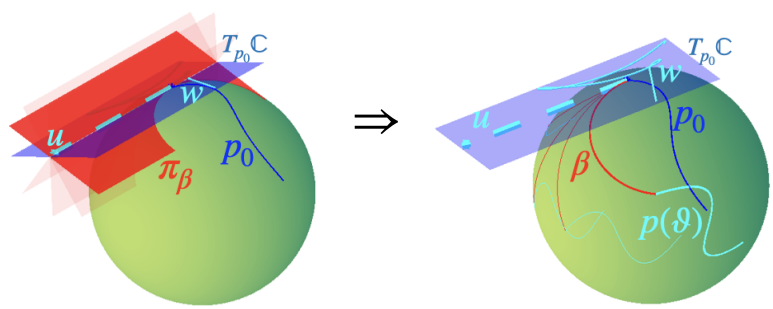

(a) (b)

Figure 19: Illustration on how to compute $\exp_{p_0}((u, w))$. Panel (a) shows a set of planes π_β containing the vector $u \in T_x\mathbb{S}^2$, and panel (b) shows $\beta(s;\vartheta)$ (the interactions between π_β and $\mathbb{S}^2$) and p which are also parameterized by ϑ.

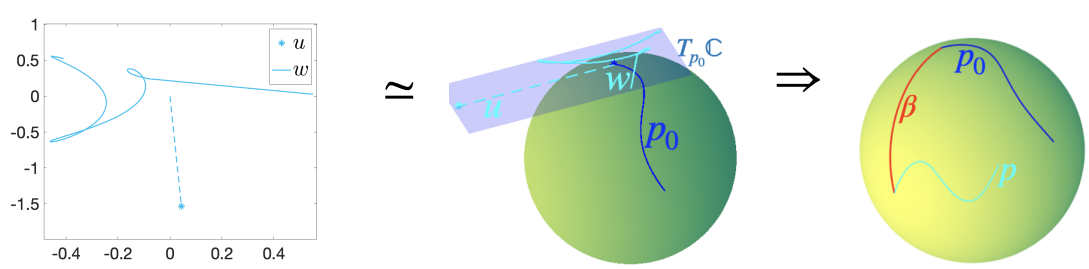

(a) (b)

Figure 20: Panel (a) illustrates an element $(u, w) \in T_{p_0}\mathbb{C}$, where u is a vector and w is a smooth function. Panel (b) shows $p = \exp_{p_0}((u, w))$ and the base-curve β.

Algorithm 7: The method for finding geodesical $\vartheta(p_0, u, w)$

Input: two smoothed functions p_0, w, the vector u, $\vartheta_0 \in \left(\arcsin\left(\frac{|u|}{\pi}\right), \pi - \arcsin\left(\frac{|u|}{\pi}\right)\right)$, the gradient step $\lambda \in \mathbb{R}$, and the degree of accuracy $\varepsilon \in \mathbb{R}$

Output: a point $\vartheta \in \left(\arcsin\left(\frac{|u|}{\pi}\right), \pi - \arcsin\left(\frac{|u|}{\pi}\right)\right)$

begin

Set $\vartheta = \vartheta_0$.

repeat

Compute $\bar{\vartheta} = \vartheta - \lambda \frac{\partial}{\partial\vartheta}\left(\frac{\partial}{\partial\theta}\left(d^2(p_0, p, \theta)\right)^2\right)$.

if $\bar{\vartheta} \in \left(\arcsin\left(\frac{|u|}{\pi}\right), \pi - \arcsin\left(\frac{|u|}{\pi}\right)\right)$ and $\left(\frac{\partial}{\partial\theta} d^2(p_0, p(\bar{\vartheta}), \theta(\bar{\vartheta}))\right)^2 < \left(\frac{\partial}{\partial\theta} d^2(p_0, p(\vartheta), \theta(\vartheta))\right)^2$ **then**

$\vartheta = \bar{\vartheta}$;

else

$\lambda = \frac{\lambda}{2}$;

until $\left|\frac{\partial}{\partial\theta} d^2(p_0, p, \theta)\right| < \varepsilon$;

By setting $s = 1$, we get the end point $p = \exp_{p_0}((u, w))$ with

$$p = (x, q) \qquad \text{where} \quad \begin{aligned} x &= x_0 \cos\phi + (n \times x_0)\sin\phi + n\langle n, x_0\rangle(1 - \cos\phi), \\ q &= (w + q_0)^{||}_{\beta}. \end{aligned}$$

Figure 19 panel (a) illustrates a set of planes π_β that contain the vector $u \in T_x\mathbb{S}^2$ (parameterized by ϑ with normal vectors in (20), and panel (b) shows $\beta(s; \vartheta)$ and p which are also parameterized by ϑ.

To this end the challenge is to find an appropriate ϑ, such that the angle $\theta(\vartheta) = \arcsin\left(\sqrt{\frac{2}{1+\langle x_0, x\rangle}}\cos\vartheta\right)$ is optimal for p_0 and p, i.e., the base-curve β gives the smallest distance between p_0 and p. We then derive a gradient decent method to find the optimal $\vartheta \in \left(\arcsin\left(\frac{|u|}{\pi}\right), \pi - \arcsin\left(\frac{|u|}{\pi}\right)\right)$. Consequently we derive Algorithm 7 to find the $\vartheta(p_0, u, w) = \operatorname{argmin}_{\vartheta \in \left(\arcsin\left(\frac{|u|}{\pi}\right), \pi - \arcsin\left(\frac{|u|}{\pi}\right)\right)} \left(\frac{\partial}{\partial\theta} d^2(p_0, p(\vartheta), \theta(\vartheta))\right)^2$.

A.5 The gradient $\nabla d^2(p0, p, \theta)$.

For further notation simplicity, given any vector $a = (a^1, a^2, a^3) \in \mathbb{R}^3$ one can expressed the cross product $a \times x$ as the multiplication of the matrix

$$(a\times) = \begin{pmatrix} 0 & -a^3 & a^2 \\ a^3 & 0 & -a^1 \\ -a^2 & a^1 & 0 \end{pmatrix} \quad \text{to the vector} x \in \mathbb{R}^3: \quad a \times x = (a \times)x$$

and the identity matrix

$$I = \begin{pmatrix} 1 & 0 & 0 \\ 0 & 1 & 0 \\ 0 & 0 & 1 \end{pmatrix}.$$

Finally we consider taking the gradient of $d^2(p_0, p, \theta)$ with respect to the second path p

$$\nabla d^2(p_0, p, \theta) = \left(\nabla_x d^2(p_0, p, \theta), \nabla_q d^2(p_0, p, \theta)\right) = \left(\nabla_x d^2(p_0, p, \theta), \quad 2\left(q(t) - q^{||}_{0,\beta(1)}(t)\right)\right),$$

where

$$\begin{aligned} \nabla_x d^2(p_0, p, \theta) =& (I - xx^T)2\phi\sin\alpha\left(\sin\alpha\nabla_x\phi + \phi\cos\alpha\nabla_x\alpha\right) \\ &+ (I - xx^T)2\int_0^1 \left(D_x\left(q^{||}_{0,\beta(1)}(t)\right)\right)^T \left(q^{||}_{0,\beta(1)}(t) - q(t)\right)\mathrm{d}t, \end{aligned}$$

with

$$D_x\big(q^{||}_{0,\beta(1)}(t)\big) = v q_0(t)^T (D_x e_2) - \big(v \times x\big) q_0(t)^T (x_0\times)(D_x e_2) + \big\langle e_2, q_0(t)\big\rangle D_x v$$
$$- \big\langle e_2 \times x_0, q_0(t)\big\rangle (x\times) D_x v + \big\langle e_2 \times x_0, q_0(t)\big\rangle (v\times),$$

for

$$D_x v = e_1\big(\nabla_x v^1\big)^T + v^1 D_x e_1 + e_2\big(\nabla_x v^2\big)^T + v^2 D_x e_2 + n\big(\nabla_x v^3\big)^T + v^3 D_x n,$$

and

$$\nabla_x v^1 = \frac{\partial v^1}{\partial \alpha}\nabla_x \alpha + \frac{\partial v^1}{\partial \phi}\nabla_x \phi, \qquad \nabla_x \alpha = -\frac{x_0 \sin\theta}{2\sqrt{(1+\langle x_0, x\rangle)(1+\cos^2\theta - \langle x_0, x\rangle \sin^2\theta)}},$$
$$\nabla_x v^2 = \frac{\partial v^2}{\partial \alpha}\nabla_x \alpha + \frac{\partial v^2}{\partial \phi}\nabla_x \phi, \qquad \nabla_x \phi = -\frac{2x_0\cos\theta}{\big(1+\cos^2\theta - \langle x_0, x\rangle \sin^2\theta\big)\sqrt{1-\langle x_0, x\rangle^2}},$$
$$\nabla_x v^3 = \frac{\partial v^3}{\partial \alpha}\nabla_x \alpha + \frac{\partial v^3}{\partial \phi}\nabla_x \phi,$$

and

$$D_x n = D_x n(x_0, x, \theta) = \frac{\sin\theta}{|x_0 + x|} I - \frac{\sin\theta}{|x_0+x|^3}(x_0+x)(x_0+x)^T$$
$$+ \frac{\cos\theta}{|x_0\times x|}(x_0\times) - \frac{\cos\theta}{|x_0\times x|^3}(x_0\times x)(x_0\times x)^T(x_0\times),$$
$$D_x e_2 = \frac{(n\times x_0)(n\times x_0)^T(x_0\times)D_x n}{\big|n\times x_0\big|^3} - \frac{(x_0\times)D_x n}{\big|n\times x_0\big|},$$
$$D_x e_1 = \frac{\big((n\times x_0)\times n\big)(n\times x_0)^T(x_0\times)D_x n}{\big|n\times x_0\big|^3} + \frac{(n\times)(x_0\times)D_x n}{\big|n\times x_0\big|} + \left(\frac{n\times x_0}{\big|n\times x_0\big|}\times\right) D_x n.$$

It is important to point out that for the optimal base-curve $\theta = \theta(p_0, p)$

$$\nabla_x d^2_{\mathbb{C}}(p_0, p) = \nabla_x d^2(p_0, p, \theta)$$

and, since $\nabla d^2_{\mathbb{C}}(p_0, p) = -2\exp_p^{-1} p_0$, we have

$$\nabla_x d^2(p_0, p, \theta) = 2\dot{\beta}(1).$$